Commissioning of a Multipass Discharge Cell for the Study of Transient Molecules of Astrophysical Interest Using the Far-IR Beamline at the Canadian Light Source

by

Aimee Bell

A thesis submitted to the Faculty of Graduate Studies of

The University of Manitoba

In partial fulfillment of the requirements of the degree of

MASTER OF SCIENCE

Department of Chemistry

University of Manitoba

Winnipeg

Abstract

The main objective of this project was to build, install and test a new direct current discharge multipass gas cell for the Far-Infrared Beamline at the Canadian Light Source (CLS). This cell was designed to generate transient molecules of astrophysical interest and was successfully used to collect high resolution rovibrational spectra of these species in the mid- and far-infrared regions (300 to 6000 cm^{-1}). The first tests involved a study of the discharge spectrum of CS_2, a precursor for the formation of astrophysically relevant chain molecules. The spectrum of CS_2 discharge showed at least six unique product species and the discharge conditions were optimized for the detection of transient molecules. These first experiments demonstrate that the objective of this project were met and it is now possible to investigate transient molecules at the CLS. Future work will involve the optimization of the production of longer chain molecules so that their far-infrared spectra can be observed for the first time.

Acknowledgements

I would like to thank my supervisor Dr. Jennifer van Wijngaarden for inviting me back to her lab to work on this project. I am very grateful for all of her guidance, support and encouragement over the past few years. I would also like to thank my committee members, Dr. Gregg Tomy and Dr. Chris O'Dea, for their feedback and interest in this project and I would also like to acknowledge past and present members of the van Wijngaarden group for their support.

I would also like to express my gratitude to Dr. Brant Billinghurst at the Canadian Light Source (CLS) for allowing me to relocate to Saskatoon for a few months to work on this project. I am grateful for all the help, support and patience he provided during that time. I would also like to thank Tim May at the CLS for his help throughout the project and for helping me get settled into Saskatoon. I would also like to acknowledge the CLS for the additional financial support I received during my time in Saskatoon.

I am grateful to everyone who helped in the construction of the new discharge cell including: Andrew Pankewycz and Lesa Cafferty at the University of Manitoba who constructed most of the parts in the main cavity; Grant Henneberg and the other engineers at the CLS who designed and built the safety-interlock plexiglass covers for the cell; Dr. A.R.W. McKellar at the National Research Council and Dr. Dennis Tokaryk at the University of New Brunswick who supplied certain parts for the cell. I would also like to thank Dr. Marie-Aline Martin-Drumel at the Harvard Smithsonian Institute for Astrophysics for her help with the initial experiments. Addtionally, I would like to thank Dr. Dennis Tokaryk (again) for his lessons in analyzing atomic transitions and the spectra of radical molecules.

Table of Contents

List of Figures

Chapter 1

Chapter 2

Chapter 3

Chapter 4

Chapter 5

List of Tables

Chapter 4

List of Abbreviations and Acronyms

CLS = Canadian Light Source

dc = direct current

FT = Fourier Transform

FTIR = Fourier Transform infrared

FTMW = Fourier Transform microwave

FWHM = full width at half maximum

IR = infrared

ISM = interstellar medium

MCT = mercury cadmium telluride

MW = microwave

SR = synchrotron radiation

Chapter 1: Introduction

The objective of this project was to commission a new dc discharge cell that could be used to generate transient molecules to be studied using synchrotron-based far-infrared (far-IR) spectroscopy. Due to the lack of available instrumentation, high resolution molecular spectroscopy in the far-IR region is not a widely used technique. As discussed in Section 1.2, reliable laboratory spectra of transient molecules are required by spectroscopists who study molecular composition in gaseous environments. A full understanding of these systems requires spectra from multiple electromagnetic regions, including far-IR which is also known as the "fingerprint region" as the transitions in this region will differentiate even between very similar species. This chapter will define transient molecules and why their presence in nature is so interesting. The later part of this chapter will go over the theory behind the spectroscopic techniques relevant to this project.

1.1 Transient Molecules

The term "transient molecule" refers to any molecular species that is short-lived in its environment relative to other species. Such species include ions, free radicals, weakly bound clusters, metastable conformers and heat sensitive species. Transient molecules, or reactive intermediates, are the driving force behind chemical reactions which is why laboratory studies of these species are essential. However, the unstable nature of transient molecules makes it difficult to prepare highly concentrated samples for these studies. Molecular spectroscopic experiments have been made possible through the development of instrumentation that can supply an adequate concentration of transient molecules on an appropriate time scale for detection. These production

techniques work by utilizing strong perturbations that force stable precursor species to undergo reactions to produce transient molecules. Examples of such techniques include pyrolysis, photolysis, laser ablation and electrical discharge.[1]

1.2 Applications to the Study of Transient Molecules

Transient molecules have been detected with spectroscopic techniques in many natural systems ranging from ecosystems on Earth to the interstellar medium (ISM) far beyond the Solar System. These techniques work by recording spectra that correspond to interactions between molecules and electromagnetic (EM) radiation (EM spectrum is shown in Figure 1.1). The nature of these interactions is discussed in more detail in Section 1.3. To identify and characterize the molecules within a spectrum, one must consult spectroscopic data collected in a controlled laboratory setting. The study of molecular composition in nature is important for understanding chemical processes and their evolution to more complex species. The detection of transient molecules in particular is crucial because, as mentioned previously, these species drive chemical reactions. The following subsections will discuss two areas of study where the detection and characterization of transient molecules nature is an important focus.

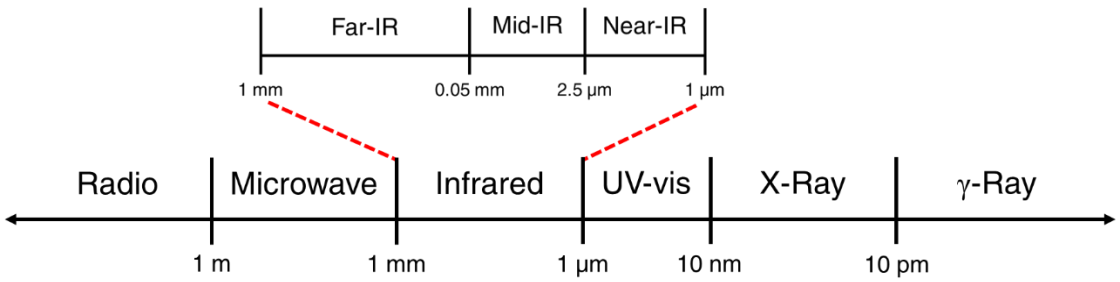

Figure 1.1: Electromagnetic Spectrum[2]

1.2.1 Atmospheric Sciences

Atmospheric scientists identify and quantify molecular species found in the Earth's atmosphere to better understand climatic phenomena, both natural and human-driven, and to measure airborne pollution levels. Precise knowledge of the Earth's atmosphere also provides criteria to astronomers and astrobiologists who seek plausible life-sustaining planets and moons. Molecules in the atmosphere can be detected spectroscopically using remote-sensing methods that detect EM radiation ranging from microwaves to ultraviolet light. Remote sensors can be placed on the Earth's surface, satellites or aircrafts.[3,4]

Many free radical species are present in the atmosphere, including OH, NO (which was observed and characterized in this project), HO_2, ClO and BrO, and are significant due to their involvement in critical chemical processes. For example, OH radicals in the troposphere (the lowest layer of the atmosphere) will convert CO to CO_2, a molecule essential to life on Earth and a greenhouse gas:

$$OH + CO \rightarrow H + CO_2$$

Meanwhile, NO radicals in the stratosphere (the area above the troposphere) are involved in the decomposition of ozone:

$$NO + O_3 \rightarrow NO_2 + O_2$$

This means that measurements of NO levels in the atmosphere can be used to track ozone levels and vice-versa.[1,4] These measurements are also indicative of air pollution levels tied to gas vehicles as NO can be released from exhaust fumes. In addition to radical species, many ions are also present in the atmosphere, particularly in the ionosphere region (altitude of >60 km). These ions

are of interest to atmospheric physicists as they are a known influence on auroras, lightning and the geomagnetic field.[4]

1.3.2 Astronomical Spectroscopy

The field of astronomical spectroscopy is concerned with the detection and identification of atomic and molecular spectra originating from various regions in space. The molecules within a detected spectrum are identified by matching spectral lines to ones collected in the laboratory. This area of study was pioneered by Robert Bunsen and Gustav Kirchhoff back in the 1860's when they were the first to realize that Fraunhofer lines in the Sun's visible spectrum actually corresponded to atomic absorption lines. They were then able to conduct the first spectroscopic study of an extra-terrestrial object by identifying atomic species in the Sun's chromosphere.[5] In modern times, astronomers can now detect emission spectra from space in almost any part of the EM spectrum. Detections of microwave and infrared radiation are especially important as these types of radiation can travel the greatest distances through space as their long wavelengths make them less prone to scattering. This is why it is possible to detect emissions from rotating, vibrating and rovibrating molecules in the interstellar medium (ISM) using telescopes on Earth.[6]

One application of astronomical spectroscopy is the study of molecules in comets. Cometary spectra can grant insight into the chemical evolution of the Solar System as comets contain many remnants from the early days of the Solar System (and possibly from before its existence). For example, the study of comets can also reveal information about the chemical diversity in the two trans-Neptunian regions where they originate from; short orbit comets come from the Kuiper belt region just beyond Neptune where Pluto is located and long orbit comets originate from the Oort cloud region at the fringe of the Solar System. Many radicals and ions

have been detected in comets through spectroscopic methods. The coloured tails of comets are actually the result of fluorescing ions generated by solar flares. The ion content of the tail will determine whether it is coloured blue (CO^+) or green (CN^+, C_2^+).[6-8]

Another popular application of astronomical spectroscopy is keeping stock of the molecular inventory in the ISM. By studying the molecular diversity of the ISM, one can gain insight into many chemical processes behind star formation and the chemical evolution of the Universe. Nearly 200 molecules have been identified so far the ISM and over 100 of these species are transient.[9] The environmental conditions in the ISM, notably the low temperatures and low gas densities, are ideal for stabilizing transient molecules. This has led to scenarios where a molecule has been detected in the ISM before any laboratory data could be recorded.[1,10] A notable example of this is C_2S which was detected in the ISM twice[11,12] before a laboratory microwave spectrum was finally recorded to allow for its identification.[13] This illustrates the importance of recording the spectra of astrophysically relevant molecules using well-resolved techniques in the laboratory. This project aims to help with the deficiency of high resolution data in the far-IR region regarding transient molecules.

1.3 Molecular Spectroscopy of Linear Molecules

The main objective of molecular spectroscopy is to better understand the physical and chemical behaviour of molecules by probing their unique energy levels related to electronic, vibrational and rotational energies. Spectroscopic studies consist of recording and analyzing spectra that display how a molecule interacts with certain types of EM radiation. Analyses of these spectra reveal information about the energy landscapes and structures of molecules. Additionally,

molecular spectra collected in a laboratory can be used to identify EM emissions from molecules in the Earth's atmosphere or the far reaches of space (as discussed in Section 1.2). This section will discuss the theory of rotational, vibrational and rovibrational spectroscopy in detail.

1.3.1 Molecular Rotation

The interaction between molecules and EM radiation in the microwave region is associated with molecular rotation (for lighter diatomic species, this can occur in the far-infrared region instead). To study these motions quantitatively, a molecule is assigned a three-dimensional principal axis system where the origin is located at the molecule's center of mass (Figure 1.2). Rotation about each axis gives rise to a moment of inertia, which is defined as:

$$I = \sum m_i r_i^2 \qquad (1\text{-}1)$$

where r_i is the distance between a mass (m_i) and the axis of rotation. The a-axis is assigned to the molecule's minimum moment of inertia, the c-axis is assigned to the maximum moment of inertia and the b-axis is placed perpendicularly to the other two to set up a right-handed axis system. This gives the moments of inertia the following relation: $I_a \leq I_b \leq I_c$. With the axis system in place, a molecular rotation can be defined as a movement of the entire molecule about an axis where a change in nuclear coordinates occurs for at least one atom while the center of mass remains fixed. Under this definition, most molecules have three modes of rotation with the exception being linear molecules which only have two modes as the rotation about the a-axis does not displace any atoms.[10,14,15]

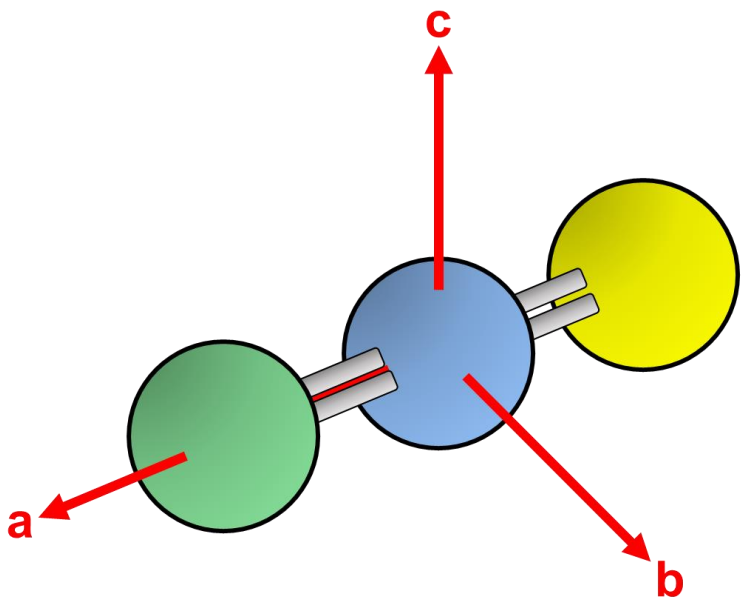

Figure 1.2: Principal Axis System for a Linear Molecule

The symmetry of a molecule will determine if the pure rotational spectrum can be recorded in the microwave region. This is because a permanent electric dipole moment is a prerequisite for detection via microwave spectroscopy and is only present in molecules with a certain degree of asymmetry. Molecules with inversion centers lack this required asymmetry and therefore have no permanent electric dipole moment. In the specific case of linear molecules, rotating species in the $C_{\infty v}$ point group (no inversion centres), such as HCN, can be detected by spectrometers but species in the $D_{\infty h}$ point group (which have inversion centres), such as CS_2, cannot. However, the rotation of $D_{\infty h}$ molecules can still be studied via rovibrational infrared spectroscopy which will be discussed in Section 1.3.3.[16]

The simplest way to model the physics of molecular rotation in a diatomic or linear species is to use the rigid rotor model from quantum mechanics which ignores the effects of vibration (v=0).[15] Using this model, quantized rotational energy levels (E_r) of a linear molecule can be expressed as:

$$E_r = \frac{h^2}{8\pi^2 I} J(J+1) \qquad (1\text{-}2)$$

Where h is Planck's constant, J is the rotational quantum number (J = 0, 1, 2, …) and E_r is in units of Joules (J). The rotational constant (B) of a rigid rotor molecule is:

$$B = \frac{h}{8\pi^2 I_B} \qquad (1\text{-}3)$$

Where B is also in units of Joules. To express B in units of wavenumbers (cm^{-1}), the units of choice in this project (for reference: 1 $cm^{-1} = 10^{-4}$ μm):

$$B = \frac{h}{8\pi^2 c I_B} \qquad (1\text{-}4)$$

Combining equations 1-2 and 1-3 gives the following rotational term value expression:

$$F(J) = \frac{E_r}{hc} = BJ(J+1) \qquad (1\text{-}5)$$

Every molecule has its own unique set of rotational energy levels, like the set seen in Figure 1.3, where the gaps between the levels are determined by the value of F(J) and labelled using quantum number J. However, real molecules are always vibrating and bonds will lengthen during rotation so a better way to express F(J) is to expand it to account for these effects:

$$F(J) = BJ(J+1) - DJ^2(J+1)^2 \qquad (1\text{-}6)$$

Where D is the centrifugal distortion constant which can be approximated as:

$$D = \frac{4B^3}{\nu^2} \qquad (1\text{-}7)$$

Where ν represents a harmonic vibration frequency in cm^{-1}.[14,17]

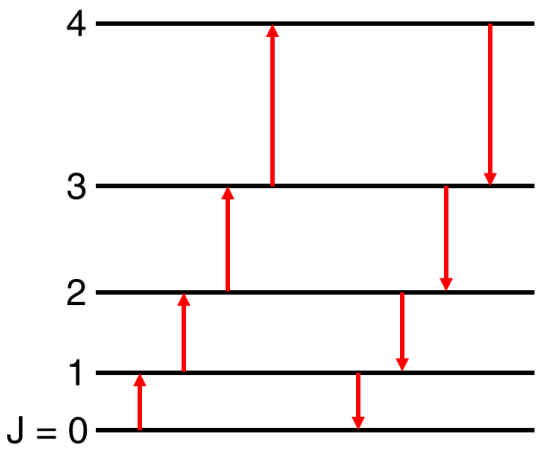

Figure 1.3: Rotational Energy Levels for a Linear Molecule (not to scale)

Under ambient conditions, a molecule will populate multiple rotational levels where the population of each level is determined by the Boltzmann distribution:

$$\frac{n_i}{n_j} = \frac{g_i}{g_j} e^{-(\varepsilon_i - \varepsilon_j)/k_b T} \qquad (1\text{-}8)^{18}$$

Where n_i/n_j is the population ratio between two states (i and j), g represents the degeneracy of each state, ε is the rotational energy value of each state, k_b is the Boltzmann constant and T is the temperature. The rotational energy of a molecule will change when quantized energy transitions occur between the different levels. For linear molecules, these energy transitions obey the selection rule of $\Delta J = \pm 1$ (As shown in Figure 1.3 above) though perturbations can allow for violations. Rotational spectra produced from the absorption or emission of microwave radiation will yield peaks located at the frequencies related to these changes in rotational energy. The relative intensities of the peaks are correlated with equation 1-8.[10,14]

The main objective when analyzing a pure rotational spectrum from microwave spectroscopy is to obtain rotational and centrifugal distortion constants. Non-linear molecules will have three rotational constants (A, B, C) corresponding to the three principal axes while linear species only have one (B) since $A = \infty$ ($I_a = 0$) and B = C.[16] Linear and diatomic molecules have

only one distortion constant represented by equation 1-6 while non-linear species will have multiple constants that are only approximately related by far more complex equations. Once determined, rotational and centrifugal distortion constants can then be used in calculations to derive structural parameters of the molecule such as bond length, bond angles and planarity.

1.3.2 Molecular Vibration

Molecular vibrations are defined as oscillatory movements that distort molecular structure, such as the stretching or bending (Figure 1.4). The number of vibrational modes per molecule is determined by the "leftover degrees of freedom". To elaborate, every atom in a molecule has three degrees of freedom before bonding is considered; one degree for each translational direction (x, y, z) of the atom. This gives 3N total degrees of freedom where N is the number of atoms. Once bonding is considered, the molecule translates as one entity and thus, three degrees are claimed by translational motions, leaving 3N-3 modes for rotational and vibrational motions of the molecule. Depending on how many inertial axes are present, two (linear) or three (non-linear) of these degrees correspond to rotational modes. The remaining degrees of freedom are therefore related to vibrational modes. This results in 3N-5 vibrational modes for linear species and 3N-6 modes for non-linear species.[15]

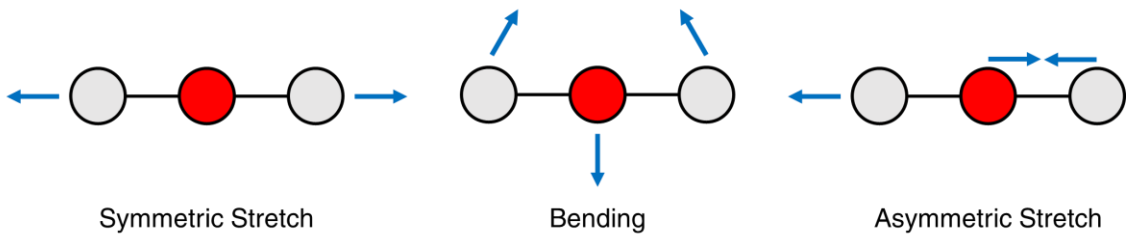

Figure 1.4: Normal Vibrational Modes for a Linear Species

(Note that this species does have four vibrational motions but two are degenerate)

The basic physics of molecular vibrations can be explained by using the stretching vibrational mode in a diatomic species as an example. In the simplest approximation, this vibration is labelled as a *harmonic oscillation* and its potential energy can be approximated using the expression for a classical spring:

$$V = \frac{1}{2}k(r - r_e)^2 \qquad (1\text{-}9)$$

Where k is the force constant and $(r - r_e)$ is the change in internuclear distance caused by the oscillation (r is the bond length at a given point in the oscillation and r_e is the equilibrium distance). The force constant is proportional to the harmonic vibrational frequency (ν), the frequency at which the harmonic vibration occurs between two masses with reduced mass (μ):

$$k = 4\pi^2\mu(\omega c)^2 \qquad (1\text{-}10)$$

The energy curve resulting from Equation 1-9 is a normal parabola that continues infinitely and gives no limits for the stretching motion. This suggests that the strength of a bond is infinite, which is not realistic for molecules. These molecules can be better represented as an *anharmonic oscillator* with a finite bond strength. The potential energy curve of an anharmonic oscillator can be seen in Figure 1.5 and may be represented by the Morse function:

$$V = D_e[1 - e^{-\beta(r - r_e)}]^2 \qquad (1\text{-}11)$$

D_e is the dissociation energy, the energy at which the bond breaks, and β is a constant proportional to ν that determines the width of the potential well.[17] Many stretching modes in polyatomic species can be represented by energy curves similar to the anharmonic case shown in Figure 1.5 while other modes, such as bending, have potential curves that are parabolas with higher order terms (quartic for example) giving narrower or wider wells. The exact shape of a potential energy curve

will depend on the structure of molecule (i.e. the curve shapes for a linear species will differ from those of a non-linear species) and this is why molecules have unique vibrational signatures.

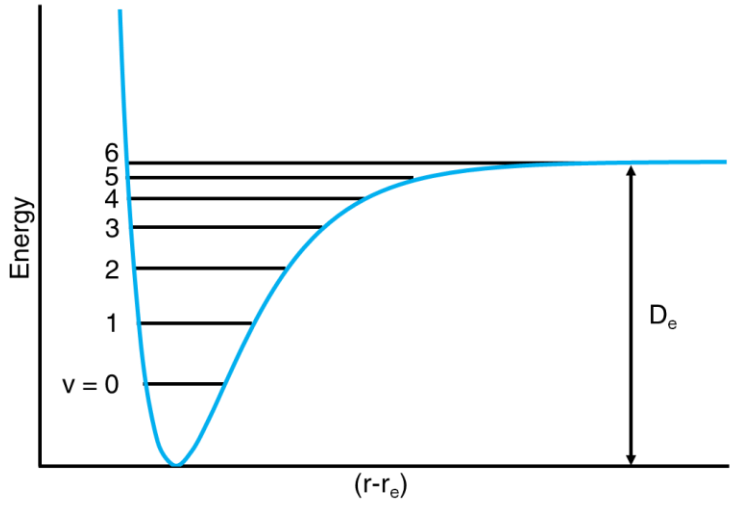

Figure 1.5: Vibrational Potential Energy Curve of an Anharmonic Oscillator

When treated with quantum mechanics (harmonic or anharmonic), the potential energy curve of a vibration contains multiple quantized energy levels labelled by vibrational quantum number v (which is not be confused with ν from before) as shown in Figure 1.5. The ground vibrational state at v = 0 is always nonzero and falls above the minimum of the curve which is why molecules are always vibrating (zero point energy), even without a prerequisite interaction with EM radiation. To transition to the higher energy levels though, an interaction with infrared radiation at a resonant frequency (ν) providing sufficient energy is required.

Vibrational transitions typically follow the quantum number selection rule of $\Delta v = \pm 1$. Spectral bands that represent $v = 1 \leftarrow 0$ transitions are known as *fundamentals* and are often the strongest bands in a spectrum. If extra energy or heat is introduced into a system, then $v = (x+1) \leftarrow x$ transitions (where $x>0$) can occur. These bands are appropriately labelled as *hot bands*. In some

cases, it is possible for the vibrational energy of two or more vibrational modes to change simultaneously which results in the appearance of *combination bands* in which the molecule will engage in two simultaneous vibrational motions. *Overtone bands* represent v = y←0 transitions where y > 1 and therefore Δv > +1.[19]

1.3.3 Molecular Rovibration

The separations between vibrational energy levels are much larger (by a few orders of magnitude) than those between rotational energy levels. As a result, a convenient way to treat these motions separately is to use a model in which each vibrational energy state has its own set of rotational energy levels (Figure 1.6). These rotational levels depend on the average geometry in each vibrational level which yield slightly different moments of inertia from those of neighbouring states for an anharmonic vibration. Interactions with infrared radiation can thus be thought of as inducing simultaneous changes to both the rotational and vibrational energy states (rovibration) but individual transitions are only detected with high resolution techniques. The basic appearance of a rovibrational infrared band for a linear species (Figure 1.7) is based on the two selection rules followed by the energy transitions: $\Delta v = \pm 1$ (vibration) and $\Delta J = 0, \pm 1$ (rotation). The P-branch represents $\Delta J = -1$ transitions, the Q-branch represents $\Delta J = 0$ and the R-branch represents $\Delta J = 1$. It should be noted that Q-branches to do not appear in for diatomic species and for certain vibrational modes in polyatomic species due to symmetry (this is discussed later). The spacing between the lines in the P and R branch are approximately equal to 2B for linear molecules.[10,14] It should be noted that Figure 1.7 is representative of an idealized spectrum; realistic spectra also contain contributions from centrifugal distortion, anharmonicity, energy perturbations and other factors discussed later in this section.

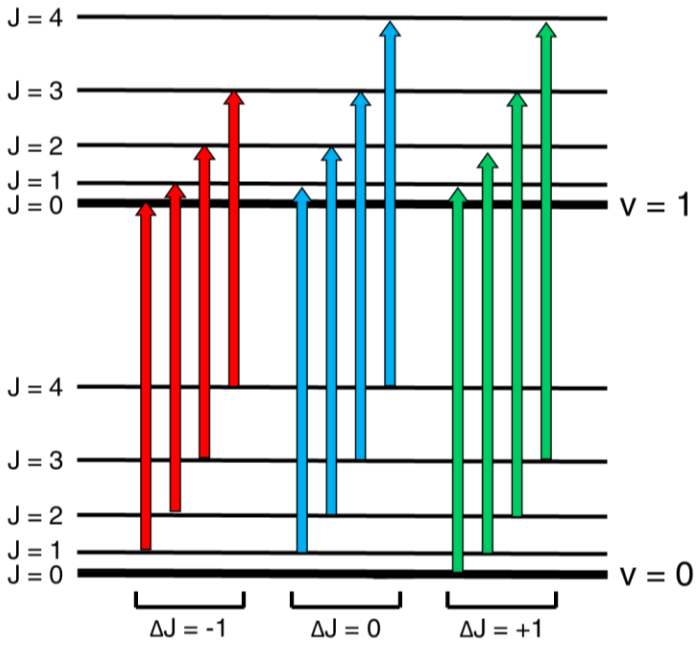

Figure 1.6: Allowed Rovibrational Transitions in a Linear Molecule (not to scale)

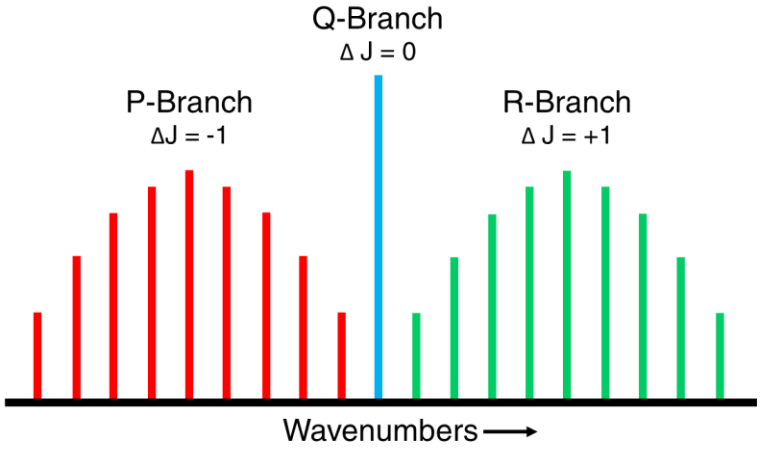

Figure 1.7: Simplified Rovibrational Spectrum for a Linear Molecule

One advantage that rovibrational spectroscopy has over pure rotational spectroscopy is the ability to study the rotation of molecules that lack permanent electric dipole moments, such as the

aforementioned $D_{\infty h}$ linear species. This is because infrared spectroscopy requires only a change in dipole moment to occur during the vibration and does not require a permeant dipole moment. By analyzing the rotational structure within a rovibrational spectrum, it is possible to generate values for rotational and distortion constants for the vibrational ground state and the excited states. The constant values determined for the ground state are the same ones that can be derived from microwave spectra if the molecule has a permanent electric dipole moment.

The changes to a molecule's electric dipole moment caused by vibration is another factor that can influence the appearance of a rovibrational spectrum. If the change in dipole moment occurs perpendicularly to the principal axis of rotation in a linear molecule, then the vibrational transition is categorized as perpendicular. If the change is parallel, then the transition is labelled as such. The vibrational motion and the rotating molecule's angular momentum (l), will determine the appearance and strength of the Q-branch in a rovibrational band. In the case of perpendicular transitions, $\Delta l = \pm 1$ which does not restrict ΔJ in any way. These bands, also known as Π-Σ transitions, will have strong Q-branches, like the one seen in Figure 1.7 above. As for parallel transitions, $\Delta l = 0$. If $l = 0$ for both the upper and lower state, then ΔJ can never equal zero which prevents the formation of a Q-branch (these are known as Σ-Σ transitions). If $l \neq 0$ for either state, then the resulting Q-branch will be weak.[16]

Figure 1.8 below shows the difference between Σ states and Π states (other types of states exist as well but are outside the scope of this project). The positive and negative signs at each rotational level represent the parity of the energy level. Rotational levels associated with Π states are doubly degenerate as $l = \pm 1$ at each level. As the molecule rotates, J and l interact which causes each J state to split into two components. This is known as l-type doubling and it is the reason

why each J value in a Π-Σ spectrum is represented as a doublet. The splitting factor (Δν) at each J level is determined by:

$$\Delta v = qJ(J+1) \qquad (1\text{-}6)$$

Where q is the *l*-type doubling constant which can be determined from a spectral analysis along with the rotational and distortion constants.[19]

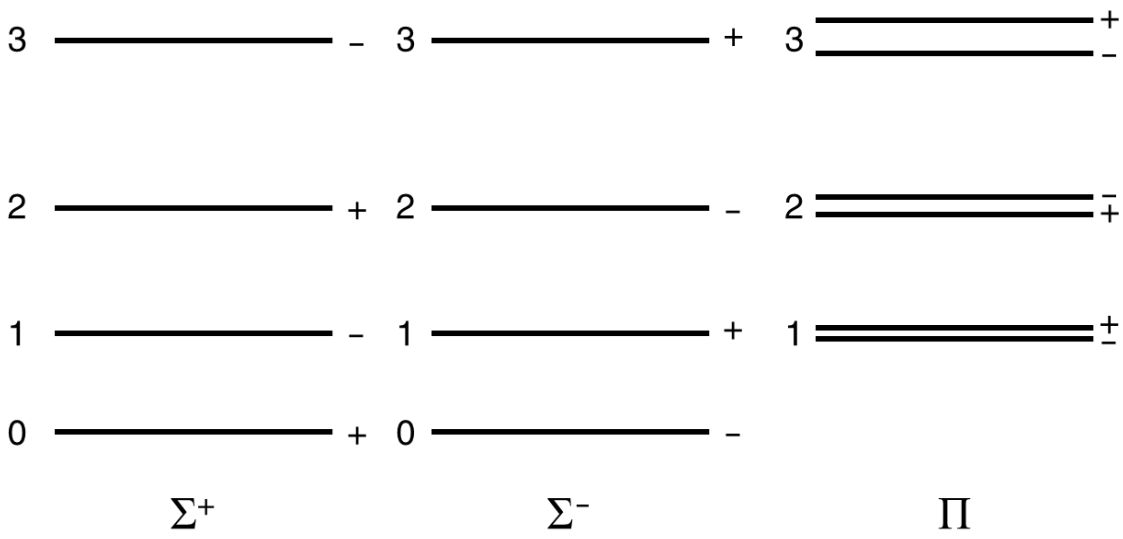

Figure 1.8: Types of Rotational States for Rovibrational Transitions (not to scale)

The next chapter will outline the spectroscopic techniques utilized in this project and the chapter after that will discuss the design of discharge cell commissioned for this project. The spectra collected with the new cell are analyzed in Chapter 4 which makes reference to much of the theory explained in this chapter. The final chapter will discuss the successes of this project and will outline some future work to be done with the new discharge cell.

1.4 References

[1] E. Hirota, *High-Resolution Spectroscopy of Transient Molecules*; Springer-Verlag: Berlin, Germany, 1985.

[2] D.A. Skoog, E.J. Holler and S.R. Crouch, *Principles of Instrumental Analysis*, 6th ed.; Thomson Brooks/Cole: Belmont, CA, USA, 2007.

[3] P.L. Hanst, Long Path Gas Cells. In *Handbook of Vibrational Spectroscopy*; P. Griffiths, J.M. Chalmers, Ed.; John Wiley & Sons, Ltd.: Chichester, UK, 2006; pp. 960-968.

[4] A.M. Holloway and R.P. Wayne, *Atmospheric Chemistry*; Royal Society of Chemistry: Cambridge, UK, 2010.

[5] G. Winnewisser and C. Kramer, *Space Sci. Rev.* **90**, 181-202 (1999).

[6] A.M. Shaw, *Astrochemistry: From Astronomy to Astrobiology*; John Wiley and Sons, Ltd.: Chichester, UK, 2006.

[7] J. Crovisier, *Mol. Phys.* **104**, 2737-2751 (2006).

[8] D. Rehder, *Chemistry in Space: From Interstellar Matter to the Origin of Life*; Wiley-VCH Verlag GmbH & Co. KGaA: Weinheim, Germany, 2010.

[9] Universität zu Köln. The CDMS Catalogue. https://www.astro.uni-koeln.de/cdms (accessed Nov 2016).

[10] J.M. Hollas, *Modern Spectroscopy*, 4th ed.; John Wiley & Sons, Ltd.: Chichester, UK, 2004.

[11] H. Suzuki, N. Kaifu, T. Miyaji, M. Morimoto, M. Ohishi and S. Saito. *Astrophys. J.* **282**, 197-199 (1984).

[12] N. Kaifu, H. Suzuki, M. Ohishi, T. Miyaji, S. Ishikawa, T. Kasuga, M. Morimoto and S. Saito, *Astrophys. J.* **317**, L111-L114 (1987).

[13] S. Saito, K. Kawaguchi, S. Yamamoto, M. Ohishi, H. Suzuki and N. Kaifu, *Astrophys. J.* **317**, L115-L119 (1987).

[14] J.M. Hollas, *Basic Atomic and Molecular Spectroscopy*; The Royal Society of Chemistry: Cambridge, UK, 2002.

[15] A. Cooksy, *Quantum Chemistry and Molecular Interactions*, 1st ed.; Pearson Education, Inc.: Upper Saddle River, NJ, USA, 2014.

[16] G. Herzberg, *Molecular Spectra and Molecular Structure II. Infrared and Raman Spectra of Polyatomic Molecules*, 2nd ed.; Krieger Publishing Company: Malabar, FL, USA, 1991.

[17] G. Herzberg, *The Spectra and Structures of Simple Free Radicals: An Introduction to Molecular Spectroscopy*; Cornell University Press: Ithaca, NY, USA, 1971.

[18] T. Engel and P. Reid, *Physical Chemistry*, 3rd ed.; Pearson Education Inc.: Glenview, IL, USA, 2013.

[19] P.F. Bernath, *Spectra of Atoms and Molecules*; Oxford University Press, Inc.: New York, NY, USA, 1995.

Chapter 2: Instrumentation for Synchrotron-Based Infrared Spectroscopy

Most molecular species have their own unique set of rovibrational transitions in the infrared region of the EM spectrum. In the case of gaseous mixtures, rotationally resolved infrared spectroscopy can be used to unambiguously identify each molecular species within the mixture without needing any sample purification. This technique is especially helpful when studying discharge chemistry. Discharge plasmas can generate a wide variety of molecular products resulting in spectra that contain many overlapping rovibrational transitions. Rotationally resolved infrared spectroscopy in the mid- and far-IR regions was the technique of choice in this project and the instrumentation that was employed is discussed in this chapter.

2.1 Fourier Transform Infrared Spectroscopy

Fourier transform techniques have made it possible to record high resolution molecular spectra. The primary component in the optics of Fourier transform infrared (FTIR) spectrometers is the Michelson interferometer (basic layout shown in Figure 2.1). This type of interferometer was developed in the mid 1880s by Nobel Laureate Albert Michelson in order to study the behaviour of light waves.[1] Michelson interferometers have since been repurposed for use in FTIR spectroscopy where they provide major advantages over traditional dispersive optics such as prisms and gratings. One of these advantages is the *Felgett advantage* which is the time saving ability to record spectral data at all wavelengths (within a region of interest) simultaneously as opposed to processing one wavelength at a time. Another advantage, known as the *Jacquinot advantage*, arises from the use of circular apertures in the optical setup that allows for more light to reach the detector than the slits used in dispersive optics.[2-4]

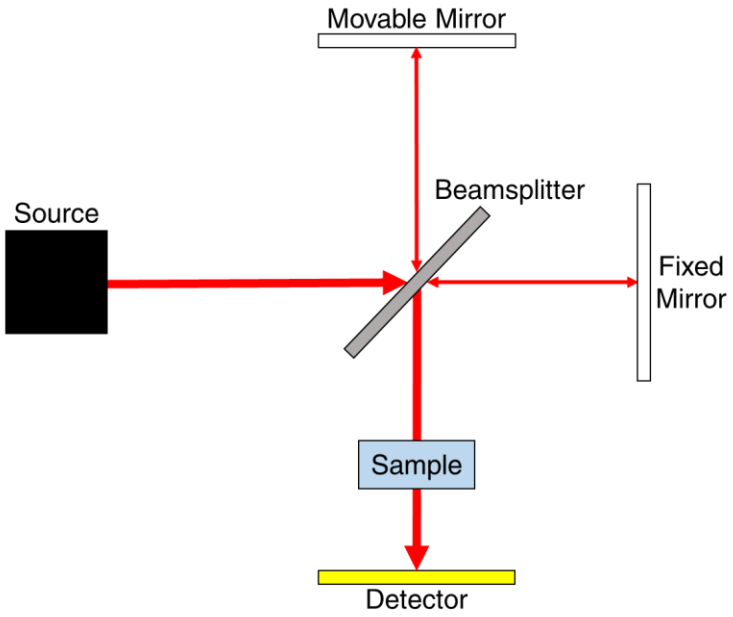

Figure 2.1: Basic Layout of a Michelson Interferometer Within a FTIR Spectrometer

The figure above shows how a Michelson interferometer is aligned within a Fourier transform infrared (FTIR) spectrometer. The process of producing an interferogram begins when infrared light is emitted from a source. In this project, a globar (heated ceramic element) was used to generate mid-IR light while a synchrotron was used for far-IR light (more details in Section 2.3). The light enters the interferometer and hits the beamsplitter where it is half-transmitted and half-reflected. The two daughter beams then travel in perpendicular directions from each other. Each beam will then reach a mirror and reflect back towards the beamsplitter where recombination occurs. However, one of the mirrors moves along a straight path during the data collection which will create a path difference (Δd(t)) between the two daughter beams that determines how they interact during recombination. The beams will constructively interfere if:

$$\Delta d(t) = n\lambda \qquad (2\text{-}1)$$

Where n is some positive integer and λ is the wavelength. Destructive interference occurs when:

$$\Delta d(t) = (2n + 1)\left(\frac{\lambda}{2}\right) \qquad (2\text{-}2)$$

The recombined beam will then travel into the sample cell and through the sample of interest if the spectrometer is set up to record absorption spectra, as it was in this project (for emission spectra, the sample cell is placed before the interferometer). Once the beam has passed though the sample cell, the infrared light will reach the detector where the intensity will be recorded as:

$$I(t) = \frac{I_0}{2}[1 + \cos(2\pi\nu\Delta d(t))] \qquad (2\text{-}3)$$

Where ν represents the wavenumber (ν = 1/λ) which is the number of wavelengths per unit length (typically in units of cm^{-1}). The data from the detector is sent to a computer that will record intensity as a function of time thus producing an interferogram.[5] However, in order to analyze the data, the time domain interferogram must be converted to a frequency domain spectrum. This can be accomplished by performing a Fourier transform on the data set:

$$F(\nu) = \int_{-\infty}^{\infty} F(t)e^{ivt}dt \qquad (2\text{-}4)$$

The above transformation is carried out using a fast Fourier transform (FFT) algorithm, typically the Cooley-Tukey method, provided by the data collection software.[6]

The resolution (Δν) of the frequency domain spectrum is affected by many variables such as optical alignment, aperture size and the movable mirror path. In the case of that last variable, the maximum path difference (Δd_{max}) between the fixed mirror and the moving mirror can limit the resolution due to the following relationship:

$$\Delta\nu = \frac{1}{\Delta d_{\max}} \qquad (2\text{-}5)$$

This means that a larger path difference allows for improved resolution.[3] Most FTIR spectrometers will have a moving mirror path lengths that span a few centimeters which restricts the resolution

to a range of 10^{-1} to 10^{-2} cm^{-1}. The Bruker IFS 125HR spectrometers that are used at select synchrotron beamlines are equipped with a 5 m mirror path (offering up to 10 m of path difference) which allows for superior resolution in the 10^{-3} to 10^{-4} cm^{-1} range.[7]

2.2 White Cells

When studying gaseous samples in the infrared region, a long absorption path is desirable for sample detection so that high pressures, which broaden molecular line widths, are not necessary. White-type sample cells (named for their inventor, John U. White) provide a way of achieving long optical paths within a compact volume of sample. The optics within these cells consist of three concave mirrors, each with identical curvature radii, that are arranged according to Figure 2.2 below. This arrangement allows for light to pass through a gaseous sample 4*n* times (*n* = positive integer). The value of *n* depends on the separation between the curvature centres of the A and A′ mirrors. The multipass capability makes excellent use of limited space; for example, a cell that is set up for 16 passes and has a separation of 1.5 m between the A/A′ mirrors and the B mirror can achieve an absorption path length of 24 m. More passes will correlate with stronger signals. Another advantage granted by the optical setup is the minimization of photon energy loss; if the mirrors are correctly set up, no light should be able to escape the cell (except through the exit window leading to the detector).[8] The only significant cause of photon energy loss in an evacuated cell is when energy is absorbed by the mirror surfaces though only the loss at the first reflection has a notable effect. The effects of energy absorption can be minimized by selecting a mirror coating with a high reflection coefficient (*R*), such as gold or silver, since the transmitted energy rate is exponentially proportional to *R*.[9]

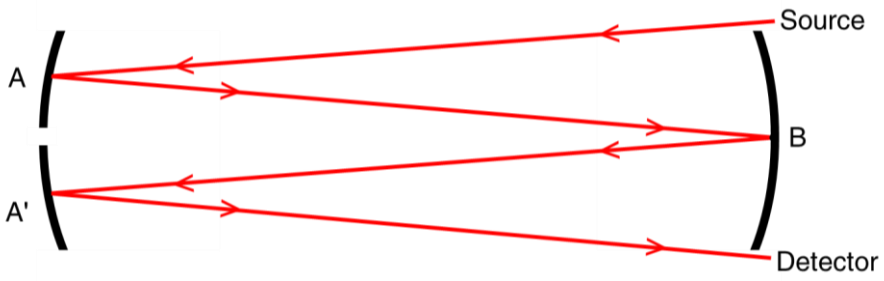

Figure 2.2: Optical Arrangement Within a White Cell

2.3 Far-Infrared Spectroscopy Using Synchrotron Radiation

Synchrotron radiation (SR) refers to the bright light emitted by a charged particle (often an electron) moving along a circular path at a constant, near-relativistic velocity.[10] There are over 50 synchrotron facilities around the world dedicated to generating and extracting SR for a variety of scientific applications. SR can be filtered to produce beams of EM radiation ranging from far-IR light to x-rays. Figure 2.3 below shows the basic layout of the Canadian Light Source (CLS), a third-generation synchrotron with a circumference of 171 m and an operating energy of 2.9 GeV.[11] The radiation process begins at the electron gun where a heated cathode emits electrons into a linear accelerator (linac). The linac will accelerate the electrons to near-relativistic speeds and pass them into the booster ring where acceleration continues along a circular track. Once a high enough velocity is reached, the electrons will move from the booster ring to the storage ring where they continue their circular trajectory. While travelling around the storage ring, the electrons will emit bright light tangentially, hence the tangential locations of the beamlines. There are devices inside the storage ring that extract the light and filter it accordingly for each beamline.[7]

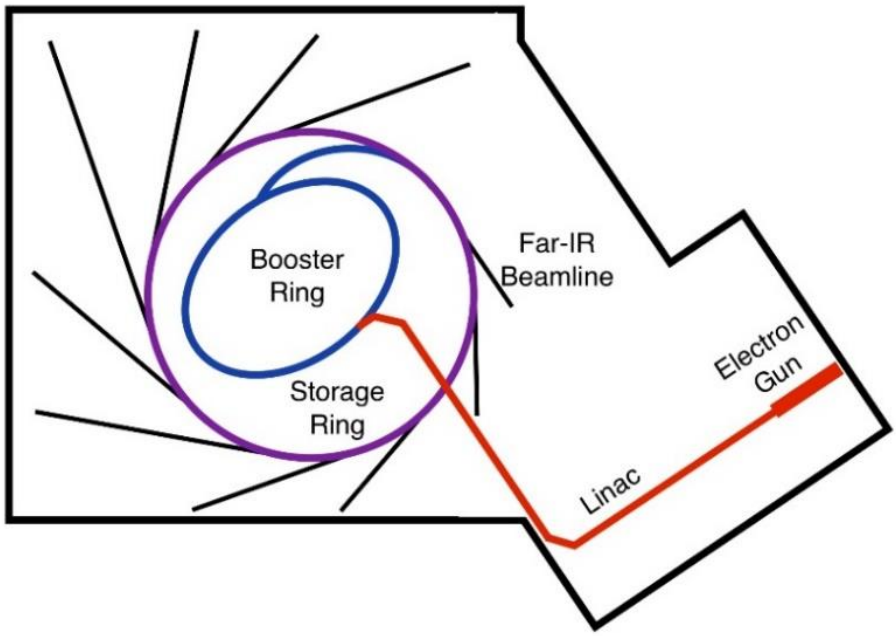

Figure 2.3: Basic Layout of the Canadian Light Source Facility

The types of devices used to extract SR will depend on what sorts of radiation are required by the beamlines. Shorter wavelength radiation (i.e. x-rays) is extracted using insertion devices, such as undulators and wigglers, placed in the straight sections of the storage ring. The extraction method for longer wavelengths, specifically far-IR, takes advantage of the previously mentioned tangential emissions. When SR is emitted at a tangent, the components of the SR will spread out at varying angles with longer wavelengths having wider angles. Bending magnets placed at the tangents in the storage ring are positioned to block out shorter wavelengths while extracting longer wavelengths. After far-IR light is extracted by these magnets, a series of mirrors will direct the light towards the beamline and focus it into the spectrometer.[7]

The far-IR light that is extracted from SR is highly collimated and contains an extremely large quantity of photons with a brightness of 4×10^{14} Photons/s-0.1%bw-mm^{2}sr.[12] This allows for beamline spectrometers to use small apertures (with diameters of 0.8 to 1.2 mm) to attain high

resolutions while still achieving strong signals due to the large number of photons reaching the detector. The use of SR is only advantageous in the far-IR region and in the mid-IR region below 1000 cm^{-1} due to the decreased Doppler widths:

$$\Delta\nu = \nu(7.1\times10^{-7})\sqrt{\frac{T}{M}} \qquad (2\text{-}6)$$

Where T is temperature and M is molecular mass. Therefore, at higher energies, the line widths of most molecules are limited by the Doppler effect and there is no advantage to using small apertures and SR. If needed, beamline spectrometers can also operate further into the mid-IR region using a globar source (data collection is must faster when using a globar source).

The use of far-IR beamlines for gas phase molecular spectroscopy has proven to be quite advantageous over traditional laboratory techniques that use mercury arc lamps[13] or laser sources. Like SR, mercury arc lamps can be used to generate radiation in any part of the far-IR region. The problem is that these lamps produce far fewer photons than SR and will emit these photons in a dispersive manner. This requires the use of larger apertures to ensure that a sufficient number of photons can reach the detector and produce noticeable signals. Unfortunately, the widening of apertures is done at the expense of resolution. Lasers are able to produce collimated IR radiation although they are quite restrictive as they are designed to work only in specific ranges as opposed to being tunable over a large range. This means that the collection of a single spectrum can potentially require multiple lasers. The ranges that can be covered by lasers are mostly in the mid- to near-IR regions; coverage in the far-IR region is quite poor.

The first known studies utilizing far-IR light from a SR source were conducted at Beamline 73 located on the MAX-I ring at the MAX-lab in Sweden. The first publication from this beamline was released in 1995 and was a study of propyne-d_1 in the 275-350 cm^{-1} region where a maximum resolution of 0.001 cm^{-1} was achieved.[14] Beamline 73 was decommissioned with the rest of the

MAX-I ring in 2015 and no replacement is planned for the new MAX-IV ring.[15] Despite the proven advantages of using SR for far-IR spectroscopy, there are currently only four synchrotron facilities in the world that have far-IR beamlines dedicated to gas phase spectroscopy and only three are open to users. The four beamlines are located at the Australian Synchrotron, the CLS, the Swiss Light Source and SOLEIL in France.[7] This project was carried out at the Far-IR Beamline at the CLS which is located at the University of Saskatchewan in Saskatoon, Saskatchewan. With the completed construction of the discharge cell in this project, it is now second far-IR beamline in the world (the first being at SOLEIL) to offer discharge experiments. Details of the commissioned cell design are discussed in the next chapter.

2.4 References

[1] Nobelprize.org. Albert A. Michelson - Facts. http://www.nobelprize.org/nobel_prizes/physics/laureates/1907/michelson-facts.html (accessed February 21, 2017).

[2] A. Cooksy, *Quantum Chemistry and Molecular Interactions*, 1st ed.; Pearson Education, Inc.: Upper Saddle River, NJ, USA, 2014.

[3] F.L. Pedrotti, L.S. Pedrotti and L.M. Pedrotti, *Optics*, 3rd ed.; Pearson Education, Inc.: Upper Saddle River, NJ, USA, 2007.

[4] W. Herres and J. Gronholz, *Comp. Appl. Lab.* **2**, 216 (1984).

[5] T. Engel and P. Reid, *Physical Chemistry*, 3rd ed.; Pearson Education Inc.: Glenview, IL, USA,

2013.

[6] A.E. Derome, *Modern NMR Techniques for Chemistry Research*, 1st ed.; Pergamon Press: Oxford, UK, 1987.

[7] A.R.W. McKellar, *J. Mol. Spectrosc.* **262**, 1-10 (2010).

[8] J.U. White, *J. Opt. Soc. Am.* **32**, 285-288 (1942).

[9] P.L. Hanst, Long Path Gas Cells. In *Handbook of Vibrational Spectroscopy*; P. Griffiths, J.M. Chalmers, Ed.; John Wiley & Sons, Ltd.: Chichester, UK, 2006; pp. 960-968.

[10] A. Hoffman, *The Physics of Synchrotron Radiation*; Cambridge University Press: Cambridge, UK, 2004.

[11] J. Cutler, E. Hallin, M. de Jong, W. Tomlinson and T. Ellis, *Nucl. Instrum. Meth. A.* **582**, 11-13 (2007).

[12] T.E. May, *Infrared Phys. Technol.* **45**, 383-387 (2004).

[13] D.A. Skoog, E.J. Holler and S.R. Crouch, *Principles of Instrumental Analysis*, 6th ed.; Thomson Brooks/Cole: Belmont, CA, USA, 2007.

[14] R. Paso and V.-M. Horneman, *J. Mol. Spectrosc.* **172**, 536-542 (1995).

[15] MAX IV. Beamlines. https://www.maxiv.lu.se/accelerators-beamlines/beamlines/ (accessed March 1, 2017).

Chapter 3: Discharge Cell Design

As one of the goals in this project was to study transient molecules using the Far-IR Beamline at the Canadian Light Source, a direct current (dc) discharge cell was designed and constructed to make these experiments possible. The design of the cell was mainly based on the hollow cathode discharge cell constructed by A.R.W. McKellar[1] (National Research Council [NRC] of Canada) that was used to study various cations and carbon chains in the mid-IR region using diode laser spectroscopy.[2-4] Some of the optical components of this cell were salvaged and reused for the discharge cell commissioned for this project. Another design influence was the dc discharge cell commissioned for the AILES beamline at SOLEIL, which was a replica of the NRC cell (minus the hollow cathode) and is used for synchrotron-based FTIR spectroscopy. This discharge cell was used to study small radical species such as OH,[5,6] CH,[5] ^{15}NH,[7] SH,[6] SO,[8] NH_2[9] and $^{15}NH_2$[10] in the far-IR region using the highest resolution offered by AILES (0.00102 cm^{-1}). As the design of the cell was intended for diode laser spectroscopy, the detection of larger transient molecules has not been possible at the AILES beamline.

The designs of the new discharge cell commissioned for this project aimed to make the cell better suited to generate larger transient species for synchrotron-based FTIR spectroscopy while also improving the durability of the cell. Such considerations included designing the dimensions of the Pyrex tube to be longer and narrower than the NRC cell, redesigning the end components to be more adjustable and innovating a way to protect the optics from discharge by-products. Details and rationale for the design of the commissioned discharge cell are discussed in the subsequent sections.

3.1 Main Cavity and Optics

The main cavity of the discharge cell can be seen in Figure 3.1 below. The primary component of the main cavity is a large Pyrex tube that was custom-built by the Glassblowing Shop at the University of Manitoba. The Pyrex tube measures at 137 cm in length, 10 cm in outer diameter and 0.5 cm in wall thickness. The narrow diameter compresses the volume of the reactant gases to reduce the minimum amount of current required to maintain a stable discharge. The electrode ports (2.5 cm in height, 1.5 cm in width) located near each end of the tube are separated by a distance of 100 cm. The long region for plasma generation between the electrodes combined with the increased density of plasma is intended to strengthen the absorbance signals of low abundance products. A stainless steel KF 40 port was placed in the middle of the cell to serve as the attachment site for the tubing that connects the cell to the vacuum pump system.

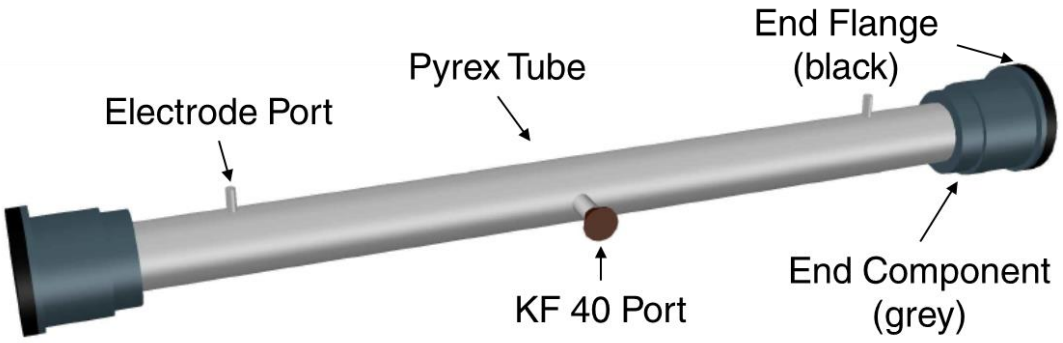

Figure 3.1: Rendering of the Main Cavity

Attached to the ends of the Pyrex tube are the aluminum end components that mate the Pyrex tube to the optics mounted on the stainless-steel end flanges. The end components were manufactured in the Machine Shop at the University of Manitoba and the end flanges were supplied by A.R.W. McKellar. As seen in Figure 3.2 below, the end components contain a series

of aluminum rings and o-rings that go around the Pyrex tube to maintain vacuum when the collars are tightened and when the cell is evacuated of air. Mounted onto the end flanges are gold coated mirrors (Figure 3.3) that are based on a design by Bernstein and Herzberg.[11] Gold works as an excellent mirror coating as it has a high reflection coefficient (*R*) of 0.98.[12] When the main cavity is fully assembled, the mirrors at each end are separated by 150 cm. The White-type arrangement of the mirrors allows for a maximum optical path length of 24 m (16 passes) within the cell. The end flange that holds the T-shaped mirror connects to the spectrometer at a port located between the interferometer and the detector (Figure 3.4). The two D-shaped mirrors, which are cut from a single circular mirror, are housed at the opposite end of the cell. Behind the T-shaped mirror are two flat KBr windows where light enters from the spectrometer (right side) and exits back out (left side). Flat windows were chosen over wedged ones as they can better tolerate changes in pressure. There are also additional gas ports located behind the mirrors on the end flanges.

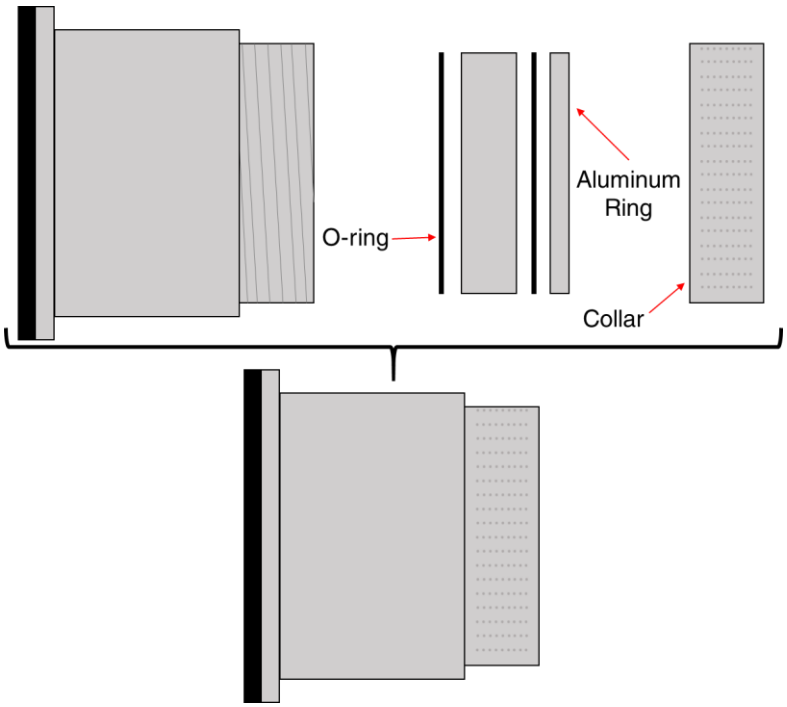

Figure 3.2: End Component Layers

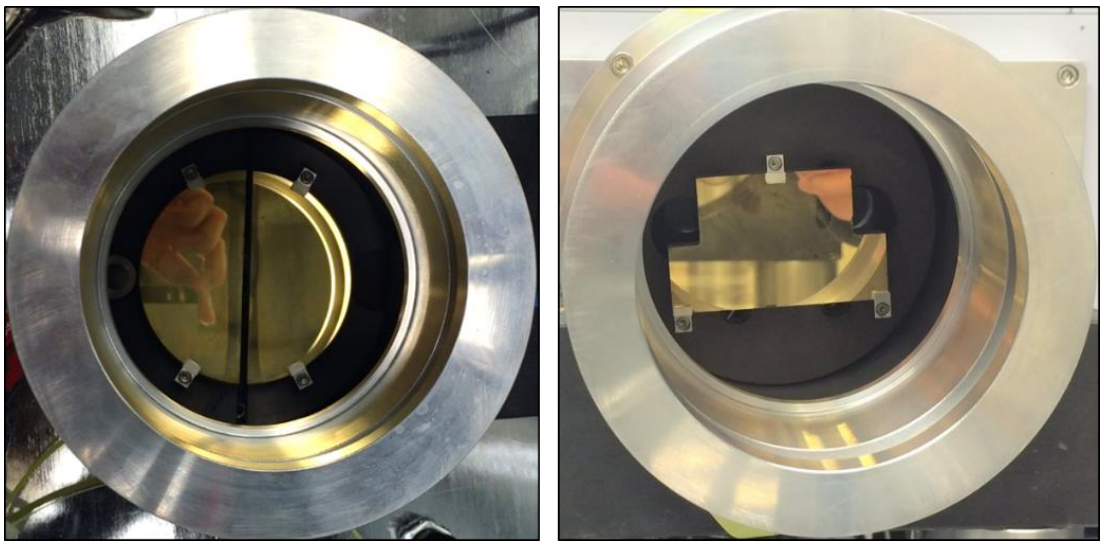

Figure 3.3: Gold-Coated Mirrors Inside the End Components

(D-shaped mirrors on the left, T-shaped mirror on the right)

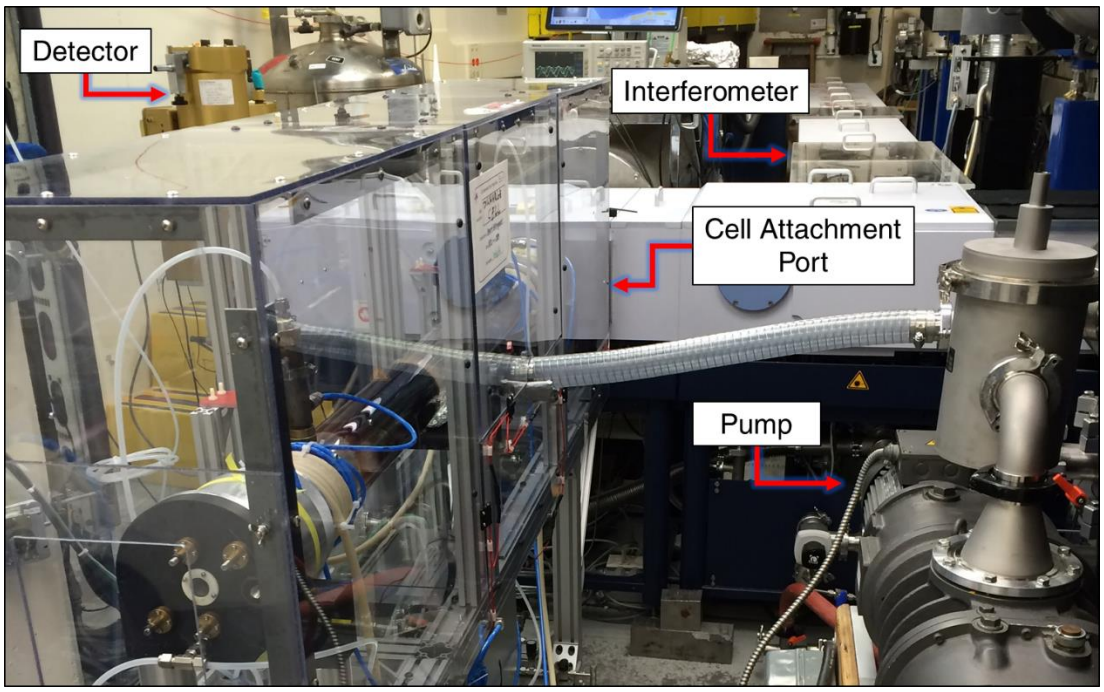

Figure 3.4: Discharge Cell Attached to the Beamline FTIR Spectrometer

3.2 Electrodes

The electrodes used for the commissioned discharge cell were supplied by D.W. Tokaryk (University of New Brunswick). Figure 3.5 below shows the layout of the connection ports on the electrodes. It should be noted that this figure shows the electrical flow within an anode; the direction is reverse in a cathode. This electrode model is comprised of two layers of stainless steel cylinders that allow for water circulation in between. The inner cylinder has a diameter of 1.5 cm while the outer cylinder has a diameter of 3 cm. The inner cylinder serves as a pathway for incoming gases; the top port of the cylinder connects to the gas line and the bottom opening attaches onto the designated electrode ports on the Pyrex tube. Only the inert gas is allowed to enter through the top port; it was observed that reactive gases were atomized by the current in the electrode since no molecular rovibrational bands could be seen in the resulting spectrum. The two side ports on the electrode are part of the outer cylinder and serve as the connection sites for the water lines. When water flows into the electrode, it will circulate in between the two layers and will cool the electrodes to prevent overheating when the discharge is running. Between the two water line ports, a high voltage wire connects the electrode to the power supply.

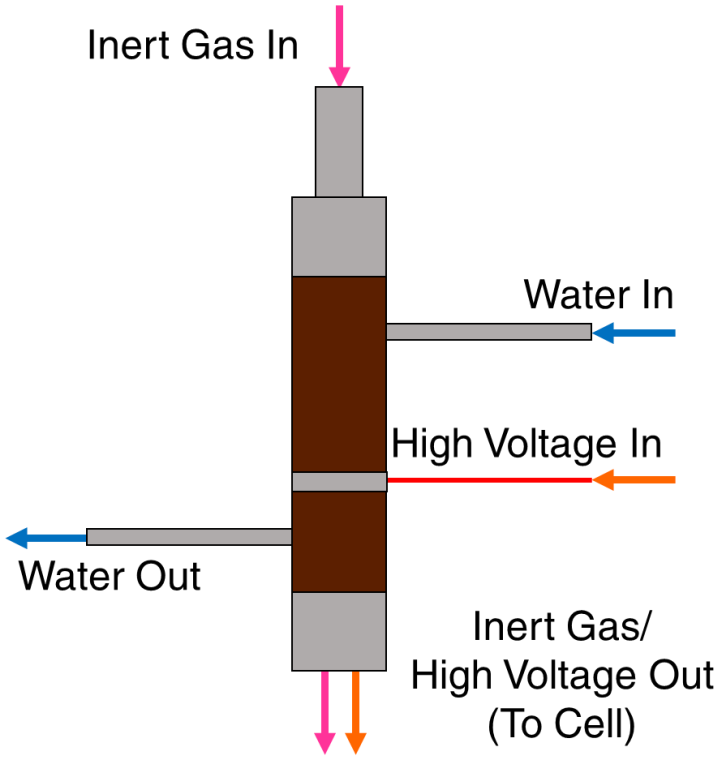

Figure 3.5: Connections for the Anode Electrode

When high voltage is applied, the electrodes become electrically live. The current flows through the cell from the anode towards the grounded cathode. The inert gas that flows into the cell through the electrodes completes the circuit between the anode and cathode. As the current flows through the gases in the cell, a plasma is generated (Figure 3.6) and chemical reactions are triggered as precursor molecules break into fragments and collide with other entities. The polarities of the electrodes must be set up so that the electrode closest to the spectrometer is designated as the cathode. If the polarities are reversed, the current entering from the anode will flow towards the spectrometer rather than the cathode as the spectrometer will be the nearest grounded object.

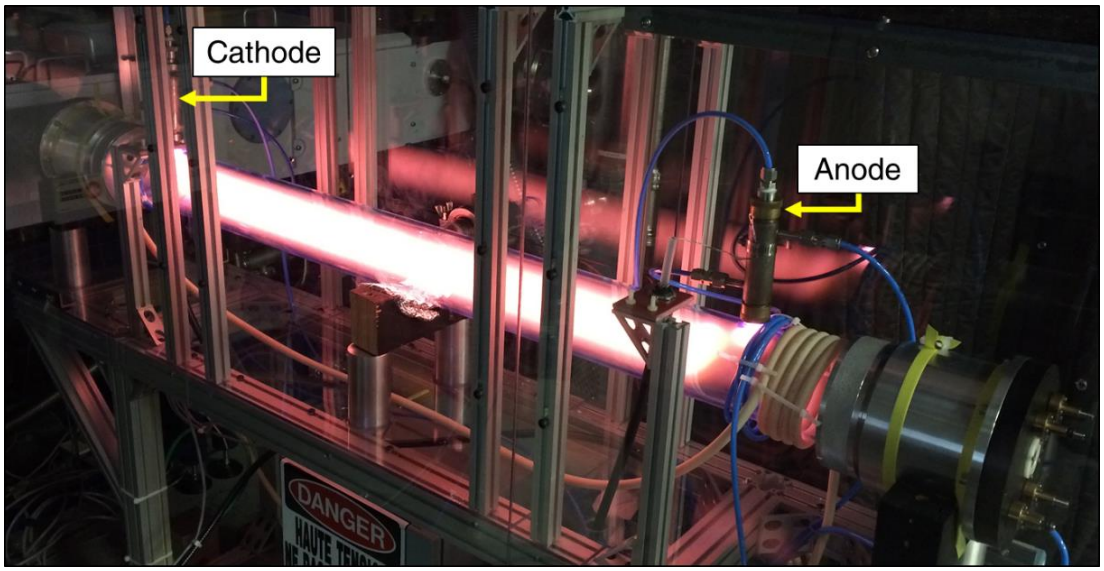

Figure 3.6: Plasma Generation in the Discharge Cell

3.3 Gas Flow

The basic setup of the gas lines and the flow of gases in the discharge cell are outlined in Figure 3.7 below. All gases enter the system at separate ports in the mixing manifold below the cell. The inert gas port has a bonnet valve since the inert gas is always set to a relatively high pressure of a few Torr and is best controlled by the gas regulator on the gas cylinder. The reactive gases are introduced at much lower pressures (up to a few hundred mTorr) so their ports are controlled by finer control needle valves on the manifold. The manifold is set up so that the inert gas is separated from the other gases although they can be mixed if needed. When exiting the manifold, the inert gas is directed through each of the electrodes while the reactive gases are sent to the gas ports on the end flanges behind the mirrors. The gas port on one of the end flanges is also hooked up to a Baratron gauge that monitors the total gas pressure inside the cell. Once the gases have entered the cell (symmetrically from each side), they are pumped through the KF 40

port in the center where they exit out of the cell. The gaseous mixture will then pass through a cold trap (cooled by liquid nitrogen) that will condense and trap hazardous by-products of the discharge. The filtered gas will then continue through the vacuum throughput system that will direct the gas into the facility's ductwork system.

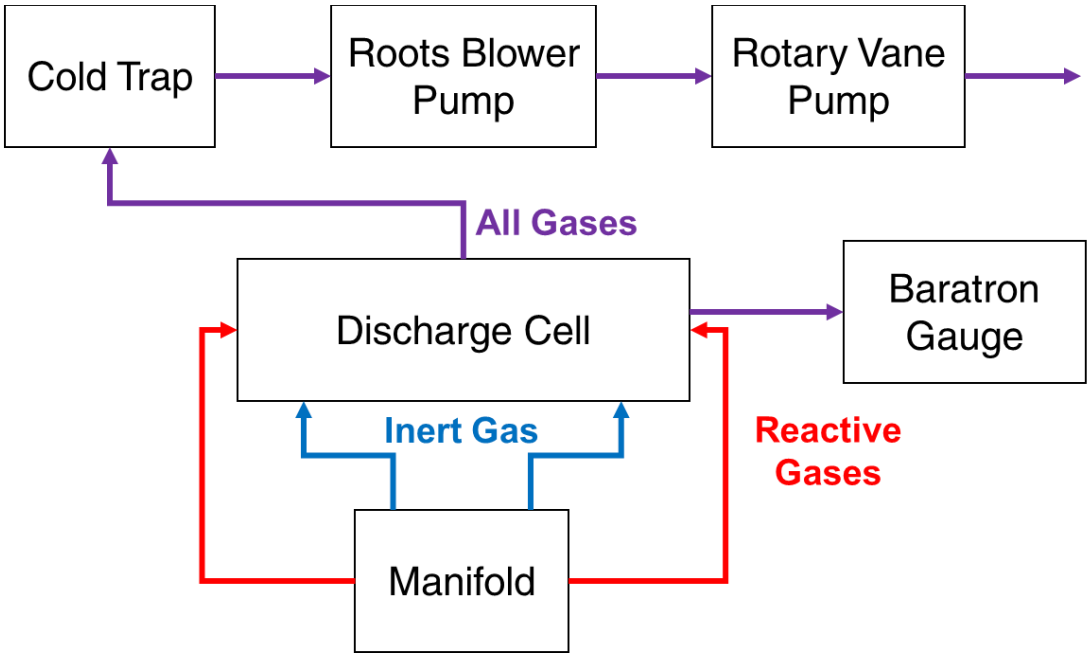

Figure 3.7: Flow of Gases Through the Discharge Cell

The vacuum throughput system of the discharge cell utilizes two separate pumps. The primary pump, located closest to the cell, is a Roots blower which is the more powerful of the two pumps. The Roots blower is usually turned on when gases are flowing into the cell though it can be shut off to reduce spectral noise. When the Roots blower is running, the pump has a tendency to generate heat which is a problem if the cold trap is in close proximity as the emitted heat can speed up the warming of the cold trap. This problem can be resolved if an insulation barrier is placed between the cold trap and the pump. The secondary pump is the rotary vane pump which

acts as a backup to the Roots blower. This pump must remain running at all times when the cell is in use, even when there are no gases flowing through the cell, in order to maintain vacuum in the cell and avoid putting stress on the windows between the cell and the spectrometer.

3.4 Mirror Protection System

When designing the discharge cell, one of the goals was to innovate a way to prevent solid buildup formed by the discharge from reaching the mirrors in the end components. This was crucial as the gold-coated mirrors are extremely difficult to clean and expensive to replace. One solution to this problem was to force the discharge products to condense in the cell before they drifted towards the mirrors. To accomplish this, Tygon (rubber) water lines were wrapped tightly around the Pyrex tube in the areas between the end components and the electrodes. A chiller was used to circulate 7 $^{\circ}$C water through the lines to cool the surface of the Pyrex tube. As seen figure 3.8 below, this innovation was successful in protecting the mirrors as the solid buildup did not reach the end components.

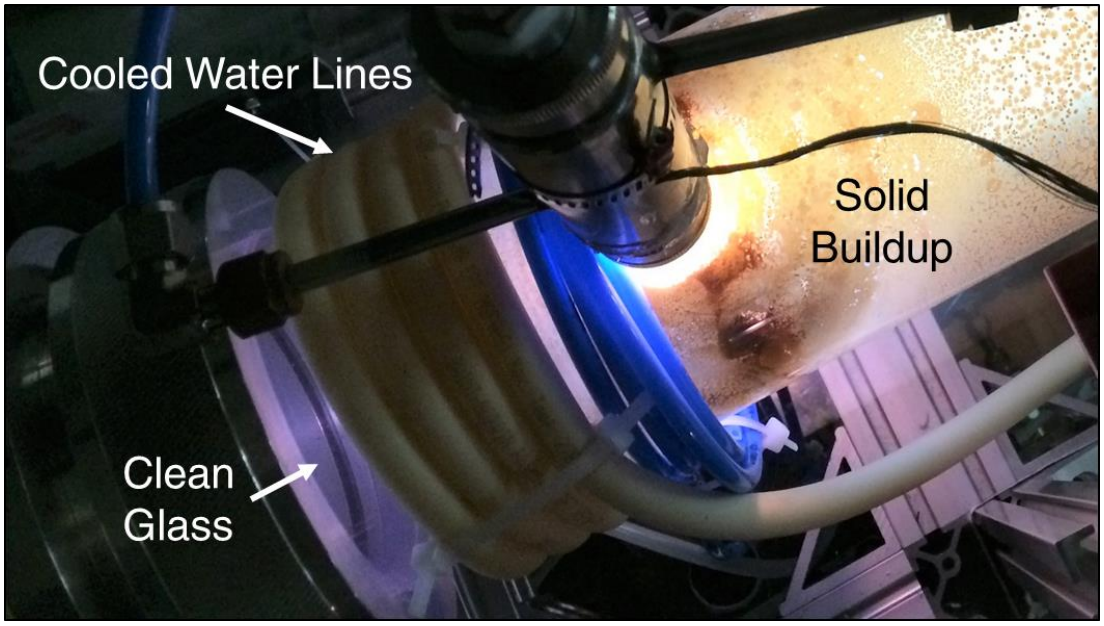

Figure 3.8: Mirror Protection System (white tubing)

3.5 Custom-Built Stand

Figure 3.9 shows the custom-built aluminum stand used to prop up the discharge cell. The cell is placed upon three wooden cradles with the aluminum end components resting on the end cradles. Since the Pyrex tube is narrower than the end components and not in contact with the middle cradle, a tinfoil cushion was placed under the tube for support. The bottom shelf of the stand is where the gas mixing manifold was mounted next to the electrical box that connects the cell to the power supply which is housed in the next room for safety reasons. The stand has wheels so that the discharge cell can be transported to and from the beamline for storage between beamtimes. When the stand is parked next to the spectrometer, a set of levelling feet can be lowered to elevate the stand so that cell is at the correct height for attachment. This also lifts the wheels off the ground so that the stand does not move while the cell is in use.

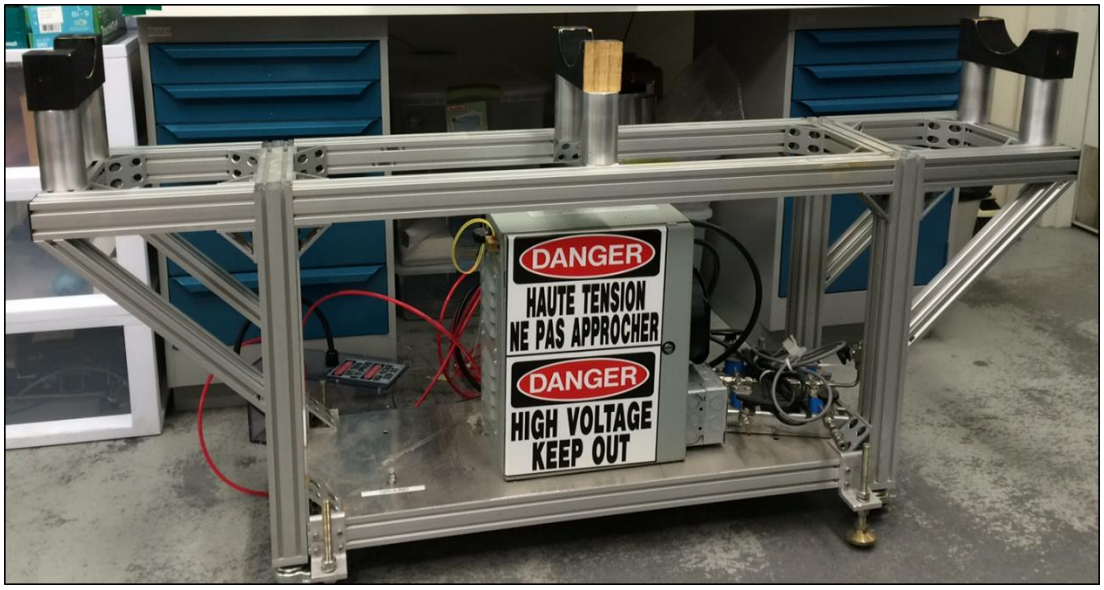

Figure 3.9: Custom-Built Stand for the Discharge Cell

The stand was constructed by modifying a pre-existing stand built, though never used, for a shorter discharge cell (the original NRC hollow cathode cell). The length of the stand was extended from 101.5 cm to 156.5 cm (adding 27.5 cm to each side) while the width was maintained at 32.5 cm. The extensions were built from Frame-World aluminum extrusions (EX-22 model), the same type of material used to construct the original stand. The extended region was set up so that the distance between the end cradles could be adjusted to better fit the cell commissioned for this project. To ensure that the end flanges maintained their 150 cm separation, the end components were strapped to the cradles to stop them from moving closer together during the gas evacuation of the cell (the yellow straps can be seen in Figure 3.6).

3.6 Safety-Interlock Plexiglass Box

As the high voltage passing through the electrodes posed an electrocution risk, the discharge cell was enclosed within a custom-built plexiglass box in order to satisfy the safety regulations imposed by the CLS. Figure 3.10 below shows the final design of the box which was done in collaboration with mechanical engineers at the CLS. The bottom face of the box is bolted to the top of stand's aluminum frame and contains small holes where electrical wires and water lines can enter and exit the box. The plexiglass piece located below the vacuum port hole is also bolted to the stand frame. The three large boxes with handles that cover the cell are all removable components that were designed so that they could be carried by a single person. The design of these three sections also allows for the adjustments to be made to the cell without having to remove all three components. The plexiglass in these sections is supported by a frame made from Frame-World aluminum extrusions (EX-11 model). When placed on the cell stand, the two end boxes rest on aluminum brackets. One of the end boxes also has an opening to allow for the T-mirror end component to attach to the spectrometer. Each component of the plexiglass box has a sensor connected to an interlock system that will shut off the power if any component of the box is removed while the discharge is running.

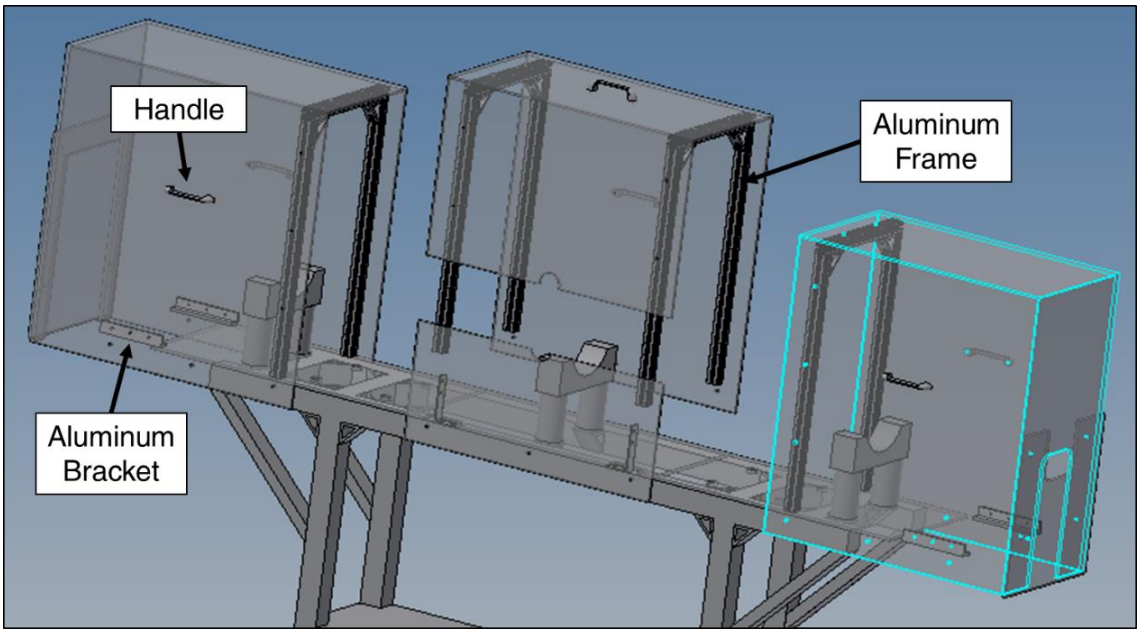

Figure 3.10: Rendering of the Plexiglass Cover

(Image Credit: G. Henneberg)

Once the discharge cell was successfully built and aligned with the beamline spectrometer, it was used to generate discharges of various chemicals (with CS_2 as the main focus) and high resolution infrared spectra of these discharges were recorded. The next chapter will explain the process of data collection and will go into a detailed analysis of the spectra collected. The final chapter of this thesis contains an evaluation of the new discharge cell's performance so far.

3.7 References

[1] S.C. Foster and A.R.W McKellar, *J. Chem. Phys.* **81**, 3424-3428 (1984).

[2] W.A. Majewski, A.R.W. McKellar, D. Sadovskii and J.K.G. Watson, *Can. J. Phys.* **72**, 1016-1027 (1994).

[3] N. Moazzen-Ahmadi, J.J. Thong and A.R.W. McKellar, *J. Chem. Phys.* **100**, 4033-4038 (1993).

[4] N. Moazzen-Ahmadi, A.R.W, McKellar and T. Amano, *Chem. Phys. Lett.* **157**, 1-4 (1989).

[5] M.A. Martin-Drumel, O. Pirali, D. Balcon, P. Bréchignac, P. Roy and M. Vervloet, *Rev. Sci. Instrum* **82,** 113106 (2011).

[6] M.A. Martin-Drumel, S. Eliet, O. Pirali, M. Guinet, F. Hindle, G. Mouret, and A. Cuisset, *Chem. Phys. Lett.* **550**, 8-14 (2012).

[7] S. Bailleux, M.A. Martin-Drumel, L. Margulès, O. Pirali, G. Wlodarczak, P. Roy, E. Roueff, M. Gerin, A. Faure and P. Hily-Blant, *Astron. Astrophys.* **538**, A135 (2012).

[8] M.A. Martin-Drumel, O. Pirali, S. Eliet and A. Cuisset, *EAS Publications.* **58**, 279-282 (2012).

[9] M.A. Martin-Drumel, O. Pirali and M. Vervloet, *J. Phys. Chem. A.* **118**, 1331-1338 (2014).

[10] L. Margulès, M.A. Martin-Drumel, O. Pirali, S. Bailleux, G. Wlodarczak, P. Roy, E. Roueff and M. Gerin, *A&A.* **591**, A110 (2016).

[11] H.J. Bernstein and G. Herzberg. *J. Chem. Phys.* **16**, 30-39 (1948).

[12] P.L. Hanst, Long Path Gas Cells. In *Handbook of Vibrational Spectroscopy*; P. Griffiths, J.M. Chalmers, Ed.; John Wiley & Sons, Ltd.: Chichester, UK, 2006; pp. 960-968.

Chapter 4: Commissioning Tests

Once the construction of the discharge cell was completed, the project focus shifted to testing and optimizing the new cell to figure out its capabilities. Of interest in the optimization was the far-IR rovibrational spectrum of CS_2 discharge products. The objective was to figure out the best discharge conditions for generating transient molecules of astrophysical interest. The testing of this new discharge cell had to be completed within the limited amount of beamtime granted by the CLS. Nearly three weeks of non-continuous beamtime was granted which gave approximately one week for each round of experiments. The setting up of the cell had to commence at least 1-2 days prior to beamtime as cell evacuation and the alignment of the optics were very time consuming. As the discharge cell could not be left to run unsupervised overnight (for safety reasons), daily experiments usually lasted no more than 10 hours.

4.1 Why Study Carbon Disulfide?

Carbon disulfide (CS_2) was selected as the reactant of interest as it has been used in previous spectroscopic studies to produce linear transient species of astrophysical interest such as C_xS chains,[1-3] HC_xS chains[4] and SCCCS[5] ($x \geq 1$). Some C_xS species have been detected in the ISM[6] and in the atmospheres of Neptune[7] and Titan[8] while HCS has been detected on Jupiter.[9] The study of sulfur-containing species in general is important in astronomy as approximately 10% of all known molecules in the ISM contain sulfur.[10] Most of the known laboratory studies of C_xS and HC_xS chains were carried out using microwave techniques to study pure rotational spectra of the chains which were formed in an electric discharge in a cold supersonic jet. The few infrared studies involving C_xS species were focused on the mid-IR region with product formation being

carried out with laser ablation rather than electrical discharge. [11-13] This means that these species have yet to be detected in the far-IR region and some of these species have yet to be successfully observed via electric discharge techniques.

4.2 Data Collection and Analysis Procedure

The experiments for this project were carried out at the Far-IR Beamline at the CLS which is equipped with a Bruker IFS 125HR spectrometer that has a moving mirror path of 5 m and a maximum resolution of 0.00096 cm^{-1}. Rovibrational spectra were collected in one of two IR regions: the 700 to 5300 cm^{-1} range (mid/near-IR) and the 450 to 1200 cm^{-1} range (far/mid-IR). For spectra in the former region, a globar source internal to the spectrometer was used to generate radiation (as the synchrotron advantage is not realized in this region) and a MCT (mercury cadmium telluride) detector was used to record spectra. SR was extracted for experiments in the latter region with the detector of choice being the GeCu bolometer. The gold-coated mirrors inside the discharge cell were adjusted so that the incoming radiation could achieve the maximum absorption path of ~24 m (16 passes) within the cell.

While the spectrometer is recording a spectrum, two averaged interferograms are uploaded to a computer every time a scan is completed (one interferogram for when the movable mirror reaches the end of its path and one for when it returns to its starting position). The incoming interferograms are received by OPUS software[14] which is then used to calculate an average interferogram from multiple scans to enhance the signal-to-noise ratio. The averaged interferogram then undergoes a FT to generate the absorbance spectrum needed for analysis. The FT command window allows for the user to choose the apodization method and the zero-filling factor (in this work, Boxcar apodization was used with a zero-filling factor of 2). The final step

in preparing an experimental absorption spectrum is to subtract the background spectrum (which should be recorded beforehand). The background spectra were recorded when the cell was evacuated at a lower resolution than the corresponding experimental spectra (as the background does not need to be rotationally resolved). Zerofilling is used to ensure that the background and experimental spectra have the same number of data points. The experimental spectrum is then exported from OPUS and converted into a format that can be opened by Pgopher,[15] the free software used for the spectral analysis in this project.

The first step in a Pgopher analysis is to generate a simulated rovibrational spectrum containing the species of interest (typically, the analysis will focus on one rovibrational band at a time). These simulations are made by entering a set of physical parameters related to the molecular Hamiltonian (rotational, vibrational and distortion constants) of the species of interest. These constants may be obtained from literature sources though *ab initio* results can be used for species that have not been experimentally characterized. With the simulations rendered, the experimental spectrum from OPUS can then be opened in Pgopher and overlaid onto the simulated spectrum. The parameters in the simulation can then be adjusted so that the vibrational center lines up with the experimental band and the rotational spacing is similar. The rotational transitions in the simulated spectrum are then assigned to peaks in the experimental spectrum. While this is a straightforward process for linear species, which are the focus of this project, it should be noted that the assignment process is far more complex for non-linear molecules. As more transitions are assigned, the parameters for the simulation can undergo a least squares fit to better characterize the molecular rotational and vibrational energy levels which will allow the simulated spectrum to better resemble the experimental spectrum. For linear species, the main parameters of interest are the vibrational center (ν_0) along with the rotational constants (B) and the distortion constants (D)

for both the ground and excited vibrational states (*l*-type doubling constant q is also generated for Π-Σ transitions). Radical species will have additional parameters to account for peak splitting arising from their unpaired electron(s). An example of a completed spectral analysis can be seen in Figure 4.1 below (note the resemblance between the simulation and the experiment). Shown in this figure is the ν_1 band system of CO (from the discharge of pure helium which is discussed in Section 4.3.1) which consists of the ν_1 fundamental band and six hot bands.

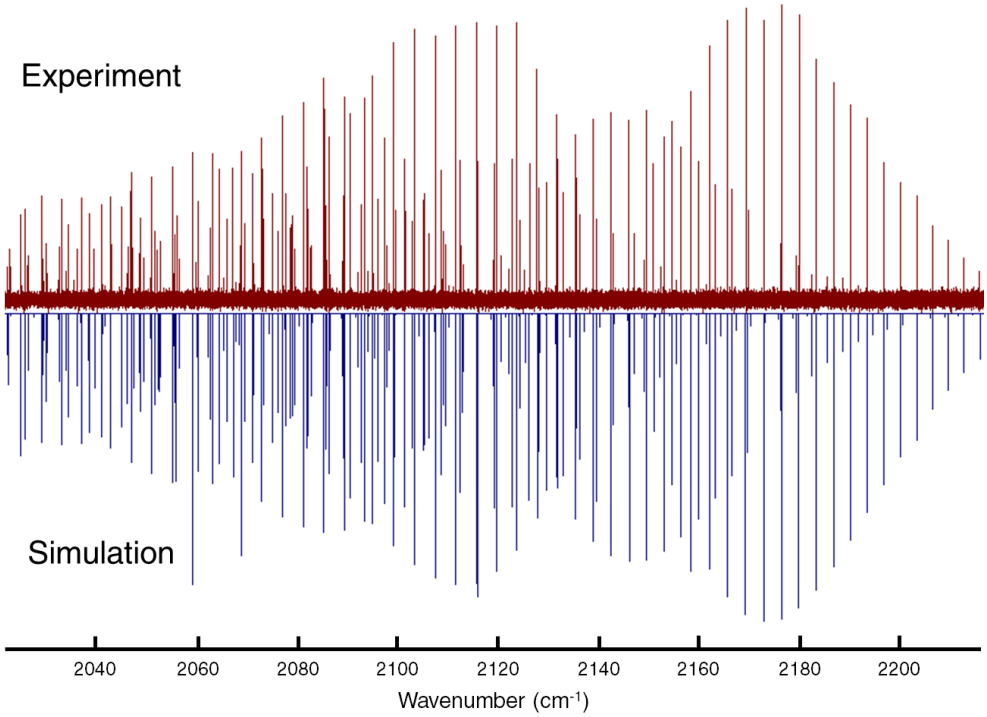

Figure 4.1: Completed Spectral Analysis of the CO Stretching Mode Using Pgopher

4.3 Early Tests

The first tests conducted with the commissioned discharge cell involved experimenting with the discharges of helium, water and air to assess the capabilities of this new cell. These

precursors were selected mainly because of their convenient availability. The spectra collected during these experiments were recorded in the wavenumber range of 700 to 5300 cm^{-1} (mid/near-IR) using the globar source and the MCT detector. The aperture size was set to 2 mm and the spectral resolution was set to 0.005 cm^{-1}. These data collection settings (globar source, larger aperture, lower resolution) were selected to keep scan times short so that more spectra could be collected within the limited amount of time granted.

4.3.1 Discharge of Helium Gas

The first set of spectra recorded with the new discharge cell focused on the discharge of pure helium gas (Figure 4.2), which was selected to be the inert carrier gas for the later CS_2 experiments (it was also the carrier gas for the water and air tests). While the discharge was turned off, the recorded spectra indicated that water vapour was entering the cell with the helium gas as indicated by two rovibrational bands corresponding to water: the ν_2 band (bending motion) at 1594.59 cm^{-1} and the ν_3 band (antisymmetric stretch) at 3755.79 cm^{-1}.[16] Once the discharge was turned on, the ν_3 rovibrational band (antisymmetric stretch) of CO_2 was observed at 2349.14 cm^{-1} and this species appeared to be breaking down into CO as evidenced by the ν_1 band (stretch) at 2143.27 cm^{-1} (Figure 4.1). The discharge was also able to further vibrationally excite the CO to produce five hot bands related to the ν_1 transition. The most surprising result was the appearance of an atomic transition of helium at 4857.45 cm^{-1} in the near-IR region. This line corresponds to the 2s ^{1}S 0 → 2p ^{1}P 1 transition of the He I atom.[17] A spectral fit of the observed rovibrational transitions of the diatomic and linear species was performed and the determined rovibrational constants can be seen in Table 4.1.

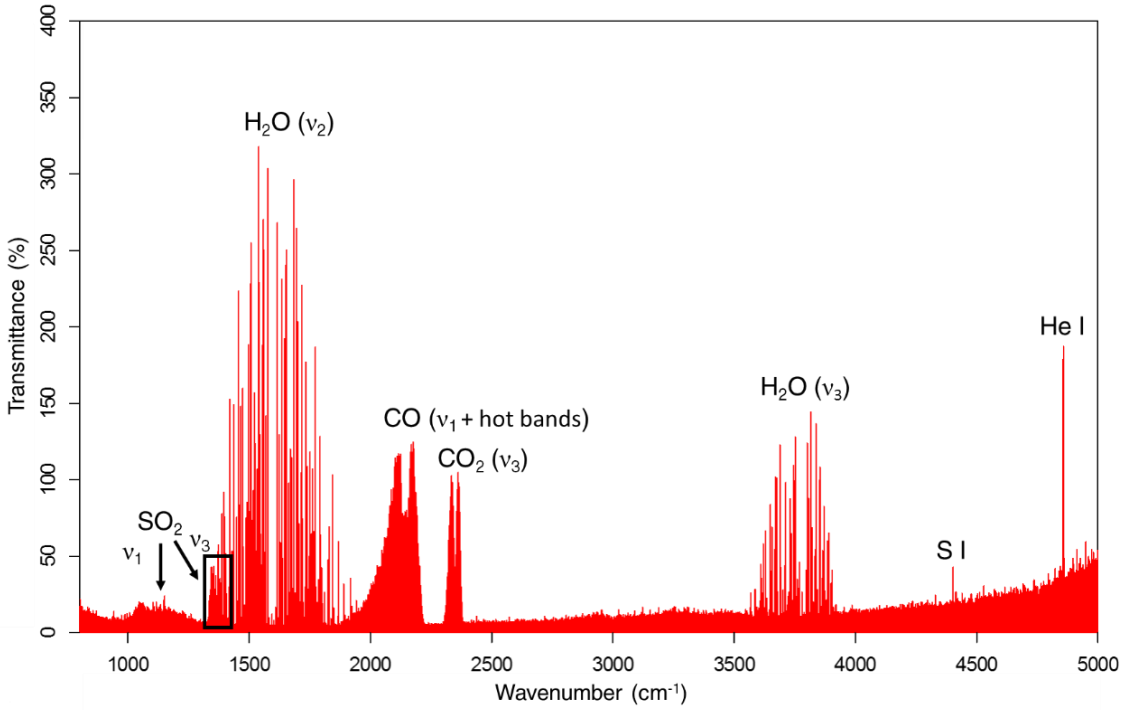

Figure 4.2: Mid/Near-IR Spectrum of Helium Gas Discharge (30 Scans)

Table 4.1: Experimental Parameters for Diatomic/Linear Species in the Discharge of Helium

	E (cm^{-1})[a]	B (cm^{-1})	D (10^6 cm^{-1})
	CO (ν_1)		
v = 0	0	1.922525(4)	6.097(6)
v = 1	2143.27056(8)	1.905024(4)	6.103(6)
v = 2	4260.0608(2)	1.887525(5)	6.119(8)
v = 3	6350.4368(3)	1.870032(5)	6.136(9)
v = 4	8414.5660(4)	1.852520(5)	6.10(1)
v = 5	10452.3182(5)	1.835013(6)	6.08(2)
v = 6	12463.8635(6)	1.817533(6)	6.61(1)
	CO_2 (ν_3)		
v = 0	0	0.390221(2)	0.1344(6)
v = 1	2349.14264(8)	0.387144(2)	0.1343(5)

[1] Hot Band Centers for CO: 2116.79024(9) cm^{-1} (v = 1 to 2), 2090.37600(9) cm^{-1} (v = 2 to 3), 2064.0292(1) cm^{-1} (v = 3 to 4), 2037.7522(1) cm^{-1} (v = 4 to 5), 2011.5453(1) cm^{-1} (v = 5 to 6)

The spectrum shown in Figure 4.2 above was collected while finding the optimal conditions for enhancing the observed atomic transition of helium. This recording took place after testing the CS_2 sample which left some solid, sulfur-containing buildup inside of the cell. When the discharge is active, SO_2 can be produced from this buildup, as shown by the presence of its ν_1 band (bend) at 1151.7 cm^{-1} and ν_3 band (antisymmetric stretch) at 1362.0 cm^{-1}.[18] Additionally, an atomic band of sulfur appeared at 4402.59 cm^{-1} which represents the 4p ^{5}P 3 → 3d ^{5}D 4 transition of the S I atom.[17] Fortunately for the optimization tests, the atomic bands of helium and sulfur had

near identical responses to changes in the discharge conditions and therefore the optimization results are applicable to both elements. During the tests, the discharge voltage and the pressure of helium were adjusted to see what settings led to the most intense atomic transitions. It was found that the most intense bands (shown in Figure 4.3) occurred at a discharge voltage of 3.50 kV and a helium pressure of 350 mTorr.

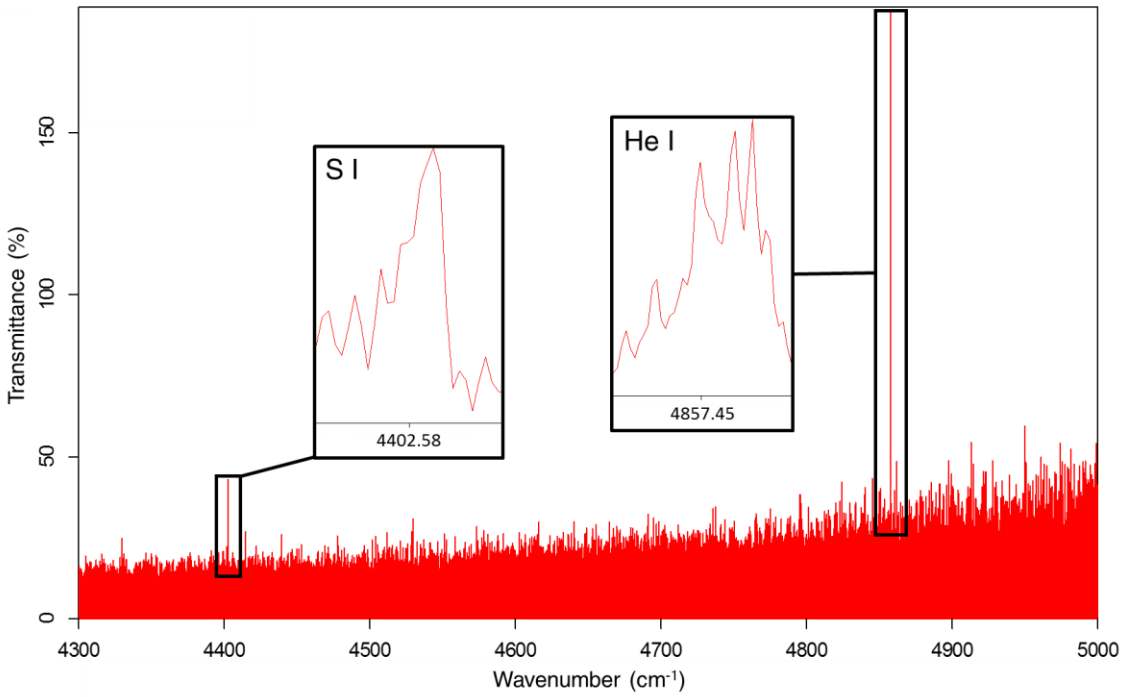

Figure 4.3: Atomic Transitions Observed in the Discharge of Helium Gas (30 Scans)

4.3.2 Discharge of Water Vapour

For the discharge of water, the goal was to produce and detect the OH radical, a difficult task due to its high instability. The conditions in the cell were set up to be similar to those used in a previous discharge study of OH that focused on its pure rotational spectrum in the far-IR region.[19] The sample pressures were set to 1500 mTorr of helium gas and 100 mTorr of water vapour. The

lowest possible stable voltage setting was used (1.30 kV) as the discharge was intended to breakdown water but not atomize it. The spectrum that resulted from these conditions can be seen in Figure 4.4 below. Unfortunately, these discharge conditions could not produce enough of the OH radical for detection (assuming it was forming at all). However, they did allow for the formation of N_2O, as shown by the ν_3 band (asymmetric stretch) at 2223.75 cm^{-1},[20] likely the product of a reaction between water and N_2 that either came from residual air in the discharge cell or was dissolved in the water sample. These discharge conditions also led to the observation of the $2\nu_2$ overtone band of water that appeared at 3151.4 cm^{-1} which is evidence that higher temperature products were generated when the discharge is turned on. Table 4.2 shows the parameters of the linear species determined from the spectral analysis in this test.

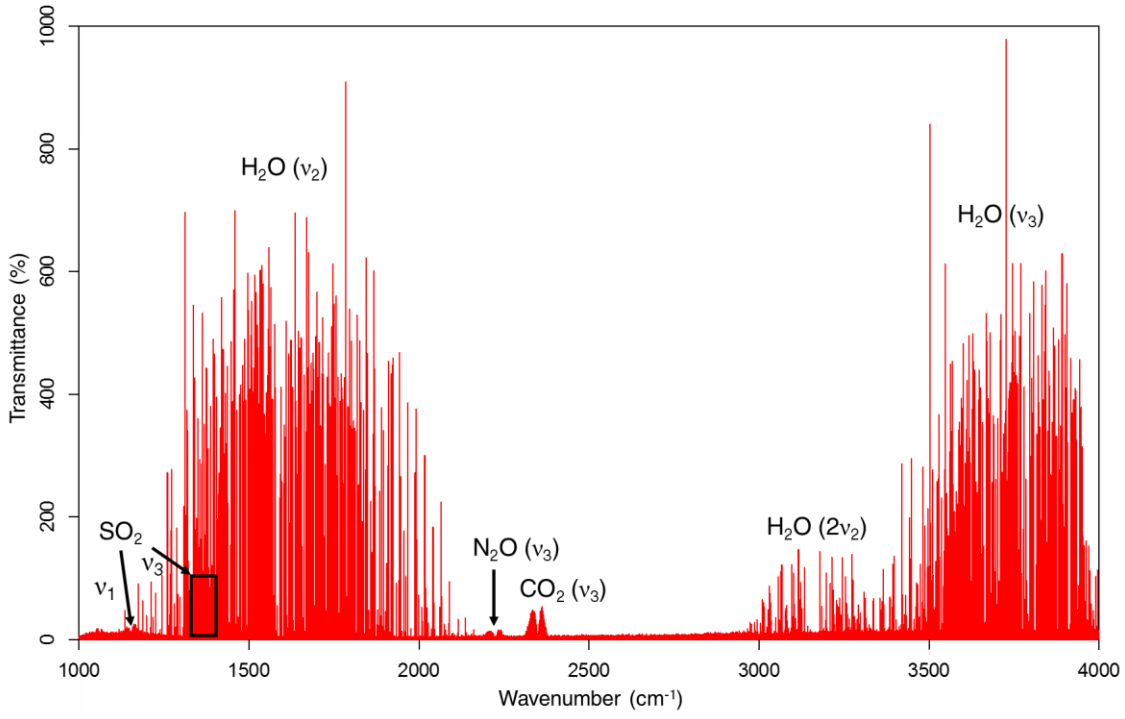

Figure 4.4: Mid-IR Spectrum of the Discharge of Water (12 Scans)

Table 4.2: Experimental Parameters for Linear Species in the Discharge of Water

	E (cm^{-1})	B (cm^{-1})	D (10^6 cm^{-1})
	N_2O (ν_3)		
v = 0	0	0.419011(4)	0.175(3)
v = 1	2223.7569(2)	0.415558(4)	0.171(3)
	CO_2 (ν_3)		
v = 0	0	0.390216(4)	0.132(2)
v = 1	2349.1429(2)	0.387138(4)	0.131(2)

4.3.3 Discharge of Air

The next round of tests was focused on the discharge of air. Since air contains multiple molecular species, its discharge was expected to generate an interesting variety of products that could showcase the capabilities of the discharge cell. The most productive spectra (in terms of molecular diversity) were produced using partial pressures of 850 mTorr of helium and 100 mTorr of air with a voltage setting of 1.50 kV. As seen in Figure 4.5 below, the resulting spectrum is evidence of a diverse range of reactions occurring in the discharge. CO_2 was broken down into CO and both species were vibrationally excited enough to allow for the observation of multiple hot bands. Additionally, the $\nu_1 + \nu_3$ combination band of SO_2 also appeared. Reactions took place between N_2 (which is undetectable due to its $D_{\infty h}$ symmetry and inability to gain an oscillating electric dipole moment from vibration) and oxygen-containing species (O_2, H_2O or CO_2) that produced N_2O (ν_1 symmetric stretch at 1284.90 cm^{-1}, ν_3 antisymmetric stretch at 2223.76 cm^{-1}) and NO (ν_1 stretch at 1875.99 cm^{-1}). The appearance of the NO radical was especially exciting as it was the first known transient species produced in the new discharge cell. The experimental

parameters for the diatomic and linear species as well as the NO radical can be found in Tables 4.3 and 4.4.

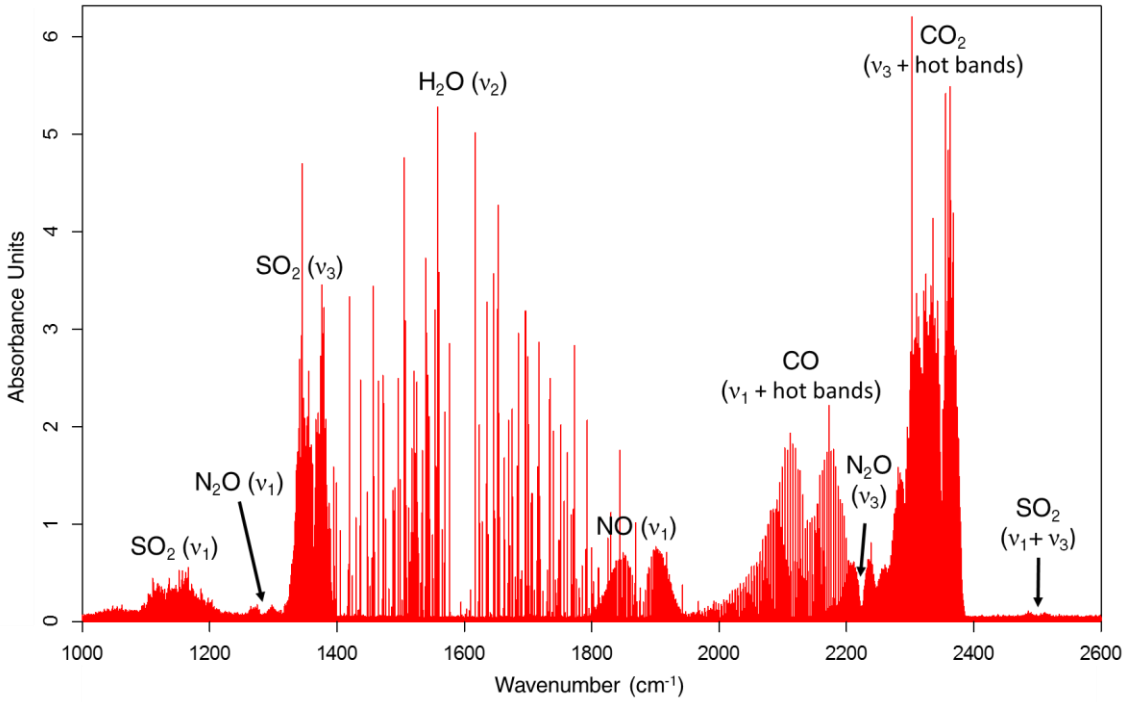

Figure 4.5: Mid-IR Spectrum of the Discharge of Air (54 Scans)

Table 4.3: Experimental Parameters for Diatomic/Linear Species in the Discharge of Air

	E (cm^{-1})[b]	B (cm^{-1})	D (10^6 cm^{-1})
	CO (ν_1)		
v = 0	0	1.922525(7)	6.10(1)
v = 1	2143.2706(2)	1.905024(7)	6.10(1)
v = 2	4260.0608(4)	1.887525(8)	6.12(1)
v = 3	6350.4368(6)	1.870032(8)	6.14(2)
	CO_2 (ν_3)		
v = 0	0	0.390216(2)	0.1325(5)
v = 1	2349.1423(1)	0.387139(2)	0.1322(5)
v = 2	4674.0927(3)	0.380990(3)	0.1324(9)
v = 3	6973.3440(4)	0.380995(3)	0.132(1)
v = 4	9246.9382(6)	0.380988(4)	0.129(1)
	N_2O (ν_1)		
v = 0	0	0.419016(4)	0.179(2)
v = 1	1284.9030(1)	0.417259(4)	0.175(2)
	N_2O (ν_3)		
v = 0	0	0.419014(3)	0.178(1)
v = 1	2223.7565(1)	0.415563(3)	0.177(1)

[b] Hot Band Centers for CO: 2143.2706(2) cm^{-1} (v = 1 to 2), 2090.3760(2) (v = 2 to 3); Hot Band Centers for CO_2: 2324.9504(2) cm^{-1} (v = 1 to 2), 2299.2513(1) (v = 2 to 3), 2273.5942(2) cm^{-1} (v = 3 to 4)

Table 4.4: Experimental Parameters for the NO Radical (ν_1) in the Discharge of Air

	E (cm^{-1})	B (cm^{-1})	D (10^6 cm^{-1})	γ (cm^{-1})	p (cm^{-1})	ΔA
v = 0	0	1.696113(4)	5.481(7)	0.0363(1)	-0.0106(1)	0.2444(1)
v = 1	1875.98890(9)	1.678541(4)	5.495(7)	0.0362(1)	-0.0106(1)	

4.4 Testing the CS_2 Sample

The main commissioning experiments in this project were focused on the discharge of CS_2 which was mixed with helium gas and air. Helium was the inert carrier gas used to help generate the discharge while air was included to act as a discharge stabilizer. If CS_2 is discharged without air, it will generate a highly unstable discharge with a lightning-like appearance that is unsafe to work with. Prior to the main experiments, a few tests were conducted with the CS_2 discharge to find out what could be observed in the spectrum and what discharge conditions should be used in the experiments. The following subsections outline how these tests were conducted.

4.4.1 Early Tests with CS_2

The first test spectra collected for the CS_2 sample used the same spectrometer settings as the test spectra of helium, water and air (see Section 4.3). At the time of these tests, there was some difficulty in stabilizing the discharge of CS_2 as a proper procedure for handling this discharge was not yet established. This meant that the discharge conditions at which spectra were collected were chosen based on the need to stabilize the discharge. The parameters that generated the most diverse spectrum (in terms of molecular species) were 2.51 kV of voltage, 2500 mTorr of helium and a combined air/CS_2 pressure of 400 mTorr. The spectrum contained many hot bands of CS_2

related to its ν_3 band (asymmetric stretch) at 1535.36 cm^{-1} and $\nu_1 + \nu_3$ combination band at 2185.47 cm^{-1} (which represents the simultaneous excitation of the ν_3 asymmetric stretch and the ν_1 symmetric stretch modes). In addition, CO_2 and CO were also vibrationally excited enough to generate multiple hot bands and buried under the CO hot bands was the ν_1 band of OCS (C-O stretch) at 2062.47 cm^{-1}. Due to spectral saturation caused by an overabundance of certain species, OCS and the hot bands of CS_2, CO_2 and CO could not be assigned in this particular spectrum. The ν_3 band (asymmetric stretch) and $(\nu_3 + \nu_2) - \nu_2$ combination hot band of the $^{13}CS_2$ isotopologue (where ν_2 represents bending) were also observed but further testing indicated that these bands were also present (and more intense) when the discharge was turned off. The discharge did manage to generate two new products that could be assigned in this region: the ν_3 band (asymmetric stretch) of HCN at 3311.33 cm^{-1} and the ν_1 band (stretch) of CS at 1272.16 cm^{-1}. The assignments for these bands are shown in Table 4.5 below and the ν_1 band of CS is shown in Figure 4.6. The observation of CS in the discharge spectrum is significant because it was the first transient species (though a relatively stable one) generated from the discharge of CS_2 in this work.

Table 4.5: Experimental Parameters for Diatomic/Linear Species in the Discharge of CS_2

	E (cm^{-1})	B (cm^{-1})	D (10^6 cm^{-1})
	CS (ν_1)		
v = 0	0	0.817077(4)	1.331(2)
v = 1	1272.1618(1)	0.811156(4)	1.333(2)
	HCN (ν_3)		
v = 0	0	1.47824(4)	2.94(8)
v = 1	3311.4782(8)	1.46780(4)	2.88(8)

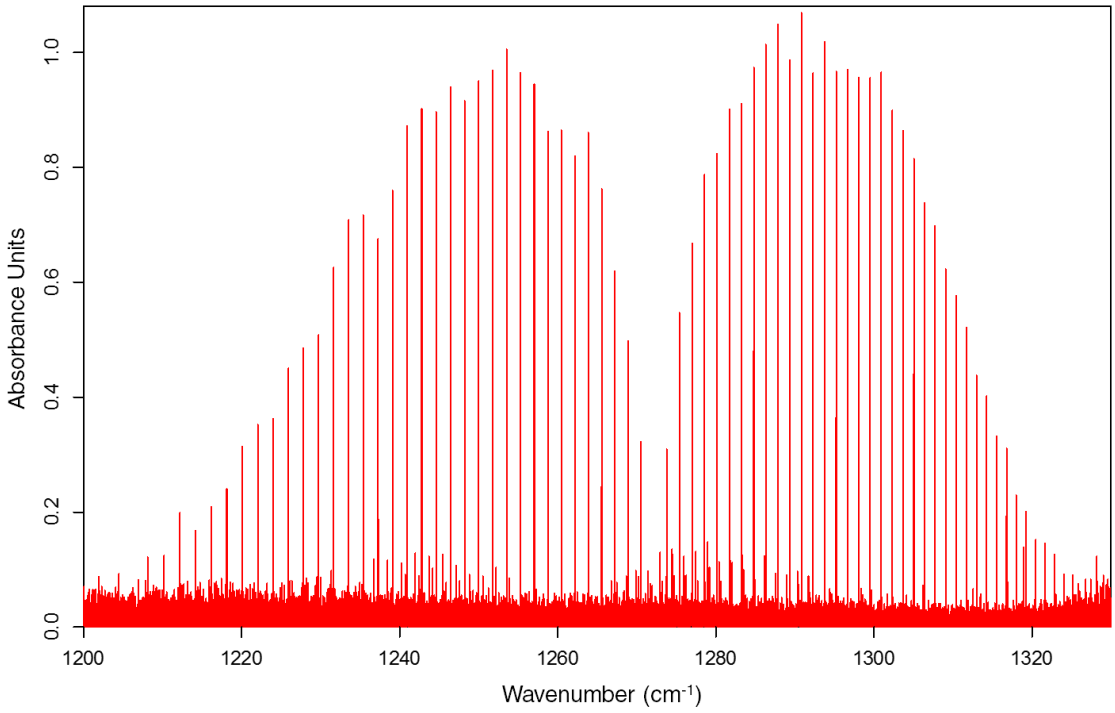

Figure 4.6: ν_1 Band of CS at 1272.16 cm^{-1} (16 Scans)

While the data analyses of spectra from the main commissioning experiment were carried out, the early test spectra of CS_2 were revisited to look for any additional species not identified during the main experiment. It turned out that one of the test spectra contained a set of bands corresponding to SCCCS, the largest species and first true linear chain molecule generated by the new discharge cell. The ν_3 band (C-S antisymmetric stretch) was assigned at 2100.10 cm^{-1} along with the $(\nu_3 + \nu_7) - \nu_7$ combination band (where ν_7 is the C-C-C bend) at 2097.65 cm^{-1} and the $(\nu_3 + 2\nu_7) - 2\nu_7$ band at 2095.18 cm^{-1}.[21] The band system can be seen in Figure 4.7 below and the determined spectroscopic constants are in Table 4.6. SCCCS was formed using a discharge voltage of 1.70 kV, a helium pressure of 2900 mTorr and a combined CS_2/air pressure of 60 mTorr. This suggests the production of SCCCS is most stable at lower voltages yet it could not be found in other lower voltage mid-IR spectra collected in a subsequent round of beamtime.

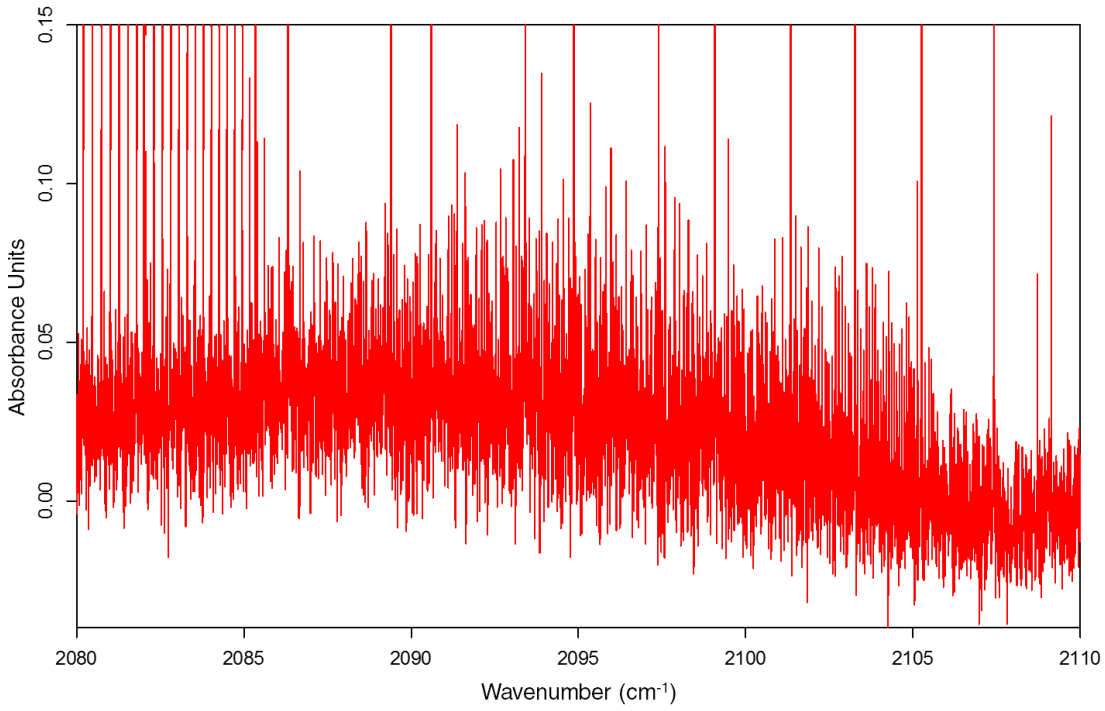

Figure 4.7: ν_3 Fundamental and Related Hot Bands of SCCCS (16 Scans)

Table 4.6: Experimental Parameters for SCCCS in the Discharge of CS_2

	E (cm^{-1})	B (cm^{-1})	D (10^6 cm^{-1})
	ν_3		
v = 0	0	0.030598(2)	0.0008(2)
v = 1	2100.0989(3)	0.030470(2)	0.0008(2)
	$(\nu_3 + \nu_7) - \nu_7$		
v = 0	0	0.030670(3)	0.0007(2)
v = 1	2097.6500(3)	0.030543(3)	0.0007(2)
	$(\nu_3 + 2\nu_7) - 2\nu_7$		
v = 0	0	0.030771(5)	0.0012(7)
v = 1	2095.1820(5)	0.030647(5)	0.0011(7)

4.4.2 Discharge Condition Tests

The objective of these tests was to systematically analyze a range of voltage and pressure settings to establish the limitations of the discharge cell and decide which settings should be used in the main commissioning experiments. For each test, the appearance of the discharge plasma was observed to see how it was affected by the changes in discharge settings. A favourable discharge is one that fills the Pyrex tube and is bright with minimal shaking and uniform in appearance which yields consecutive interferograms that are consistent in appearance over a suitable time scale. Instabilities, such as dullness or shakiness, in a discharge lower the signal-to-noise ratio and thus, require longer data acquisitions. The discharge settings that produced favourable discharges were taken into to consideration for the main experiment.

The first round of tests focused on the effect of the voltage setting on the discharge and aimed to find out the minimum amount of voltage needed to maintain the glow of the discharge. For these tests, only helium was flowed through the cell for simplicity as the carrier gas is always the most abundant component of an experiment. The voltage settings that were tested spanned a range of 0.30 kV to 3.60 kV (increments of 0.20 kV). The systematic tests were conducted at three different pressure settings for helium: 550 mTorr, 900 mTorr and 2500 mTorr. For the 550 mTorr and 900 mTorr settings, a minimum voltage of 0.40 kV was required to generate a discharge while 0.60 kV was needed for the 2500 mTorr setting. However, the discharges generated at these minimum settings were very dull. In all three cases, a voltage of at least 1.40 kV was needed to obtain a bright and stable discharge so this was therefore designated as the minimum voltage for the subsequent experiments. Figure 4.6 shows a comparison between a dull discharge and a bright discharge at the 550 mTorr of helium setting. Above 1.40 kV, the discharge appearance remains nearly the same regardless of the voltage setting, though the brightness does slowly increase with the voltage.

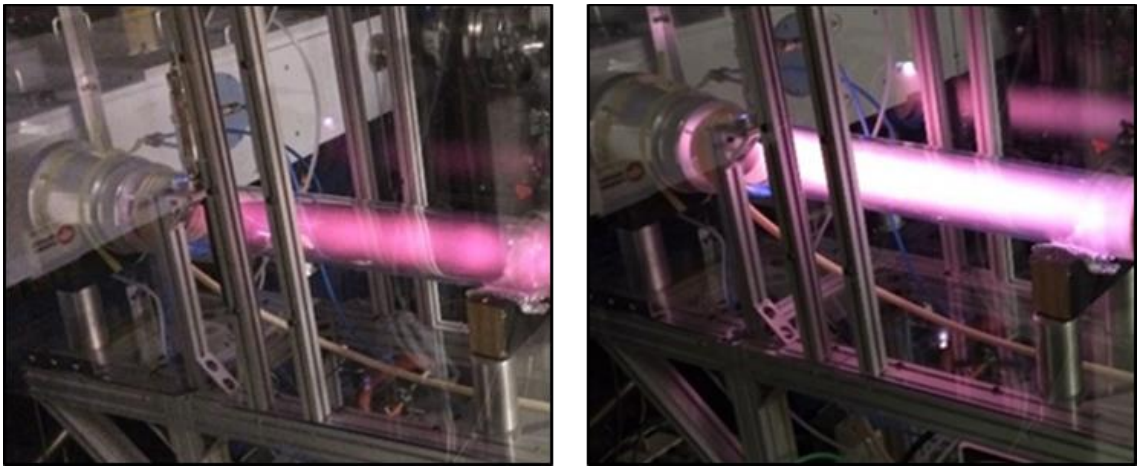

Figure 4.8: Discharge at 0.40 kV (left) and 2.00 kV (right) using 550 mTorr of Helium

The next set of tests focused on finding the optimal pressures for each component of the experimental gas mixture (CS_2, air and helium). First, the pressure of helium alone was tested at a voltage of 2.00 kV over a range of 100 mTorr to 4700 mTorr (starting at increments of 100 mTorr then gradually increasing to increments of 1000 mTorr). It was found that favourable discharges were generated in the range of 400 mTorr to 3000 mTorr of helium. Below 400 mTorr, the discharge exhibited instability and above 3000 mTorr, the discharge started to dull. The change in helium pressure also affects the discharge colour which indicates changes in the chemistry of the contaminants in the cell (discharge colour is a result of electronic excitations in the visible region of the EM spectrum). The discharge is purple below 200 mTorr, peach-pink from 400 to 2100 mTorr and orange at 2900 mTorr and higher.

The pressure of air was optimized at a voltage of 3.00 kV with the helium pressure set to 2000 mTorr (the voltage was raised to keep the discharge more stable). The air pressure was tested over a range of 0 to 1000 mTorr (increments of 100 mTorr). It was found that the pressure of air should not go above 400 mTorr as the discharge will lose stability and brightness. Keeping the voltage at 3.00 kV, the pressure of CS_2 was tested with the helium pressure set to 2000 mTorr and air pressure set to 300 mTorr. The tests were conducted over a range of 0 to 100 mTorr of CS_2 (increments of 10-20 mTorr). The most favourable discharges were achieved when the pressure of CS_2 was set below 30 mTorr. Above 30 mTorr, the discharge gradually becomes shakier, which causes an increase in spectral noise, and the discharge colour changes from pink to white due to the increase of CS_2 in the cell (Figure 4.7). Additionally, the volume of discharge also decreases near the electrodes (look closely at the reflections in Figure 4.7). Even with the reduced stability, the discharge is still stable enough for experiments at CS_2 pressures as high as 100 mTorr. However, higher pressures risk the formation of the dangerous lightning discharge. During these

tests, it was discovered that the best method for adjusting CS_2 pressure is to solely use the manifold valve instead of switching between that valve and the sample vial stopper. As discussed in the next section, the amount of CS_2 added cannot be optimized solely based on the visual appearance of the discharge as one must check the spectra to prevent oversaturation of rovibrational bands.

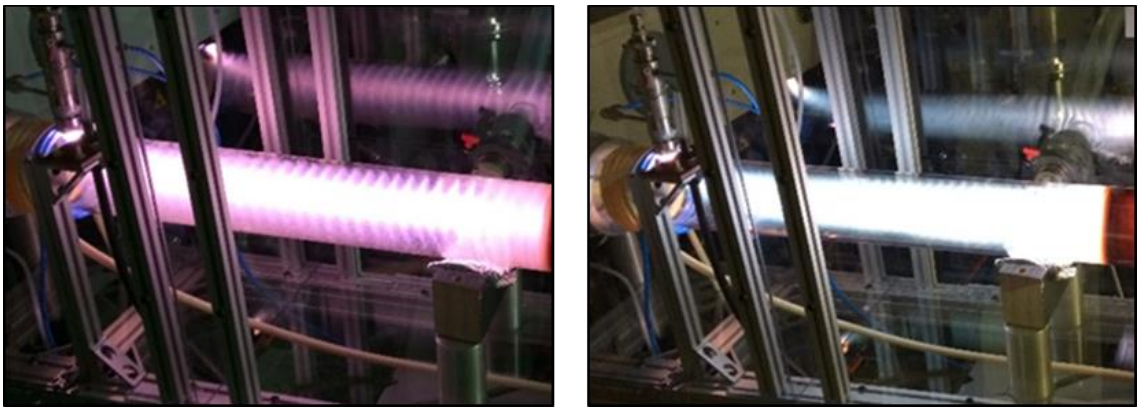

Figure 4.9: Discharge at 20 mTorr of CS_2 (left) and 100 mTorr of CS_2 (right)

4.5 Main Commissioning Experiments

The objective in the main commissioning experiments was to establish how manipulating discharge conditions affect spectra and to find the optimal conditions for producing transient molecules of astrophysical interest, specifically chain molecules, using CS_2 as a precursor. The discharge conditions of interest included the discharge voltage, the pressures of the reactive species (CS_2 and air) and the pumping rate. The spectra recorded for each change to the discharge conditions were analyzed to see what linear products could be observed and how the characteristics of rovibrational bands (intensity, line widths, number of lines, maximum J value) were affected by the changes.

4.5.1 Spectrometer Settings and Mid/Near-IR Experiments

Experiments were conducted in two different spectral regions: 700 cm^{-1} to 5300 cm^{-1} (mid/near-IR) and 450 cm^{-1} to 1200 cm^{-1} (far/mid-IR). The spectrometer settings used in these experiments are shown in Table 4.7. However, due to experimental problems encountered during the spectral recordings of the mid/near-IR, the results from that region will not be discussed here in detail. The main problem encountered during those recordings was the repeated saturation of the rovibrational bands of CS_2 and CO_2 that could not be removed no matter how the discharge conditions were changed, whether it be a change in voltage or a reduction in air or CS_2 pressure. The high level of saturation prevented these bands (and others nearby) from undergoing spectral analysis. With only a few days of experimental time, it was not possible to diagnose why the spectra seemed unresponsive to changes in discharge conditions but fortunately, these issues did not persist in the far/mid-IR experiments conducted in the next round of beamtime a few weeks later.

Table 4.7: Spectrometer Settings for the Commissioning Experiments

	Mid/Near-IR Spectra	Far/Mid-IR Spectra
Recording Range	400 to 6000 cm^{-1}	300 to 1200 cm^{-1}
Beamsplitter	KBr	KBr
Detector	MCT	GeCu Bolometer
Source	Globar	Synchrotron
Resolution	0.003 cm^{-1}	0.00096 cm^{-1}
Aperture Size	1.5 mm	1.15 mm
Gain	A	16x
Window Type	KBr	KBr
High Pass Filter	Open	1
Low Pass Filter	80	10
Electronic Filter	N/A	150 Hz/300 Hz[c]
Velocity	40 kHz	80 kHz

[c] The electronic filter had to be switched from 150 Hz to 300 Hz during the experiments to restore the signal as it suddenly reduced to half strength for unknown reasons (fortunately this happened in between spectral recordings)

4.5.2 Default Spectrum in the Far/Mid-IR Region

The experiments conducted in the far/mid-IR region were successful and provided some conclusive information. The first task in these experiments was to record a "default spectrum" to act as a benchmark for later spectra. The discharge condition settings for this spectrum were as follows:

- Discharge voltage = 3.50 kV
- Helium Pressure = 2400 mTorr

- Air Pressure = 300 mTorr
- CS_2 Pressure = 100 mTorr
- Pumping Rate: Normal Throughput

The rovibrational bands observed in the default spectrum using the above settings are listed in Table 4.8 and most of them can be seen in Figure 4.10. For each of the later spectra, one of the above conditions was changed (except helium pressure) to see how the spectrum was influenced.

Table 4.8: Rovibrational Bands Observed in the Default Far/Mid-IR Spectrum

Species	Rovibrational Bands Observed
CO_2	$2\nu_2 - \nu_2$ (618.03 cm^{-1}), (642.39 cm^{-1}),[d] (654.87 cm^{-1}),[d] ν_2 (667.38 cm^{-1}), $2\nu_2 - \nu_2$ (667.75 cm^{-1}), $\nu_1 - \nu_2$ (720.81 cm^{-1})[22]
HCN	ν_2 (711.98 cm^{-1})[23]
OCS	ν_1 (858.97 cm^{-1}),[22] $2\nu_2$ (1047.04 cm^{-1})[24]
CS_2	$\nu_1 - \nu_3$ (877.36 cm^{-1})[25]
SO	ν_1 (1138.01 cm^{-1})[26]

[d] The vibrational mode labels for these two non-fundamental bands of CO_2 have yet to be found.

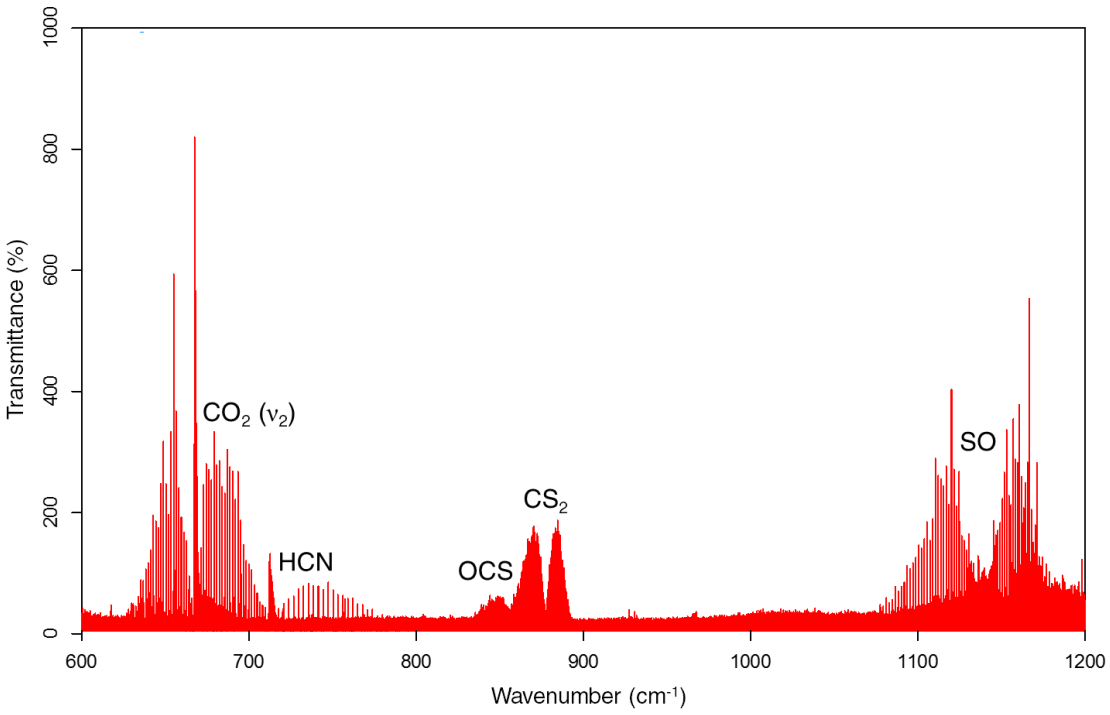

Figure 4.10: Far/Mid-IR Spectrum Generated from the Default Discharge Settings (100 Scans)

4.5.3 Overview of the Analyses in the Far/Mid-IR Region

In addition to the default spectrum, four more spectra were recorded, each representing a different change to the discharge settings. Two spectra were recorded for changes to the pressures of the reactive precursor species: one for the reduction of air pressure and the other for the reduction of CS_2. The purpose of these spectra was to figure out how the abundance of each product relied on the amount of each precursor. Another spectrum was recorded when the discharge voltage was reduced to compare the stability of the products at the different settings. The last spectrum represents the discharge when the pumping rate in the cell is reduced to half throughput. As a reduced pumping rate allows for the gaseous sample to stay in the cell longer, it was believed that this setting could help with the detection of less abundant species. All four

spectra were qualitatively analyzed for changes to molecular diversity and band intensities. Table 4.9 below shows an overview of the results from this analysis.

Table 4.9: Qualitative Overview of the Effects of Changing Discharge Conditions

	Reduced CS_2	Reduced Air	Reduced Voltage	Reduced Pumping Rate
Increased			OCS	CO_2, SO
New			C_2H_2	
Decreased	CO_2	CO_2, OCS, SO	SO, CO_2 (hot)	OCS, CS_2, HCN
Gone	OCS, HCN, CS_2			
Unchanged	SO	HCN	HCN, CS_2, CO_2 (ν_2)	

The spectra for the reductions in voltage and pumping rate underwent a more rigorous quantitative analysis, in addition to the qualitative one. Along with the default spectrum, the quantitative analysis focused on the five bands that appeared in all three spectra: CO_2 (ν_2), HCN (ν_2), OCS (ν_1), CS_2 (ν_3 - ν_1) and SO (ν_1). Each band underwent a spectral analysis using Pgopher to find the number of observable lines, the highest observable J value and the most intense J value. It was also revealed via Pgopher by simulating the spectrum at various temperatures that the temperature in the cell (with the discharge turned on) was approximately 350 K for each experiment. The full width at half maximum (FWHM) of representative lines were measured to check whether the temperature (as the discharge voltage was adjusted) or pressure (as the sample mixture was adjusted) were affecting the observed line widths. Table 4.10 shows the full list of values generated in this analysis (except for the FWHM values which will be discussed later in this paragraph). The number of lines and the highest J value are affected by both the abundance

of molecular species as well the temperature of the sample. The J quantum number values of the most intense lines in the P and R branches are influenced by temperature as this is related to the population distribution in the rotational levels of the ground state via the Boltzmann distribution (discussed in Chapter 1). When compared with the lines in the default spectrum, it was found that a change in discharge conditions caused minor, inconsistent changes to the FWHM values. For some bands, lines in the P-branch and lines in the R-branch underwent opposite changes to their FWHM values. As seen in the example of Figure 4.11, the J =10 line in the HCN band did not change consistently with the voltage reduction; it's width increased slightly in the P-branch yet decreased slightly in the R-branch. This suggests that these settings do not strongly influence line width. For this reason, the FWHM values will not be taken into account when discussing the quantitative analysis as the maximum intensity locations can provide sufficient information.

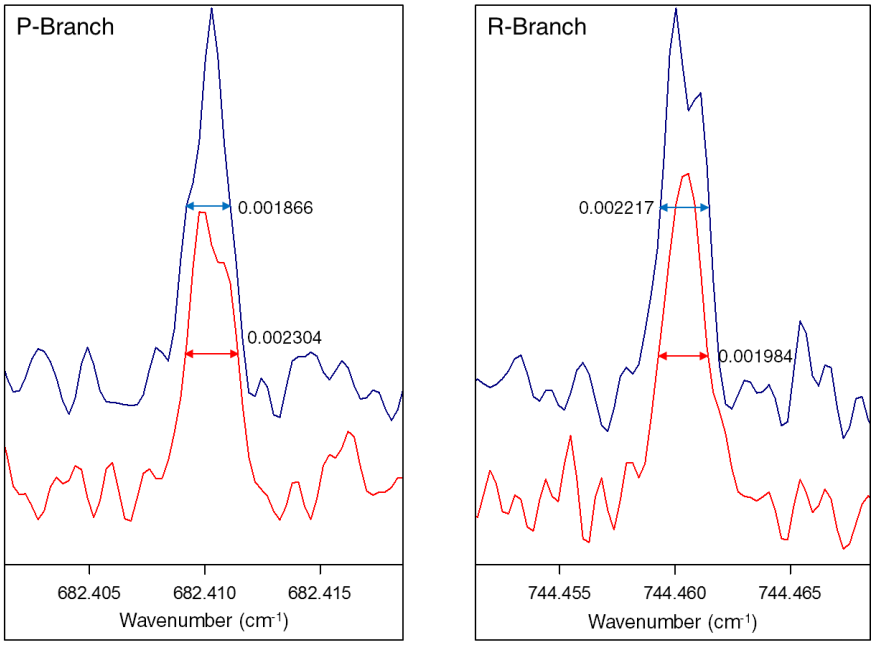

Figure 4.11: Comparison of FWHM of the J = 10 Line in HCN

(blue = default settings, red = reduced voltage)

Table 4.10: Quantitative Analysis of the Effects of Changing Discharge Conditions

	Default	Low Voltage	Reduced Pumping
	CO_2 (ν_2)		
# of Lines	47	65	*
Max J (P/R)	56/58	54/56	62/64
Most Intense J	18	18	22
	HCN (ν_2)		
# of Lines	41	42	33
Max J (P/R)	22/22	22/22	16/20
Most Intense J	10	8	8
	OCS (ν_1)		
# of Lines	100	115	78
Max J (P/R)	55/56	63/60	48/49
Most Intense J	24	26	16
	CS_2 (ν_3 - ν_1)		
# of Lines	89	92	67
Max J (P/R)	90/94	92/90	72/76
Most Intense J	32	24	28
	SO (ν_1)		
# of Lines	191	129	*
Max J (P/R)	38/30	36/32	40/30
Most Intense J	18	15	14

*Due to saturation, the number of observable lines cannot be reliably measured.

4.5.4 Effects of Precursor Pressure Changes (Far/Mid-IR)

For the two spectra recorded with reduced precursor pressures, one was recorded with the pressure of CS_2 reduced from 100 mTorr to 0 mTorr and the other with the pressure of air reduced from 300 mTorr to 150 mTorr. Comparisons between these spectra and the default spectrum can be seen in Figures 4.12 and 4.13. An attempt was made to record a spectrum with the pressure of air reduced to 0 mTorr but the discharge destabilized into a dangerous lightning-like form after ~10 minutes. The few scans that were recorded resulted in a very noisy spectrum that could not undergo a meaningful analysis. Predictably, the reduction of air in the sample led to the decrease in intensity of the rovibrational bands of all oxygen-bearing species (OCS, CO_2, SO) yet the HCN band (which was believed to be receiving nitrogen from the air) was nearly unchanged. The removal of CS_2 led to disappearance of OCS and HCN while the SO band remained almost unchanged. These results show that OCS was the product of a reaction between CS_2 and an oxygen-bearing component of air. As for HCN, CS_2 was likely the primary source of the carbon, rather than CO_2, and the nitrogen may have been provided by a contaminant in the CS_2 sample. The formation of SO was thought to be a product of a reaction between air and CS_2 but its appearance in the spectrum showing the removal of CS_2 suggests that air may have been reacting with the solid-buildup in the cell instead. It is possible that SO is formed from the breakdown of SO_2 which was confirmed to be formed in the reaction between air and solid-buildup.

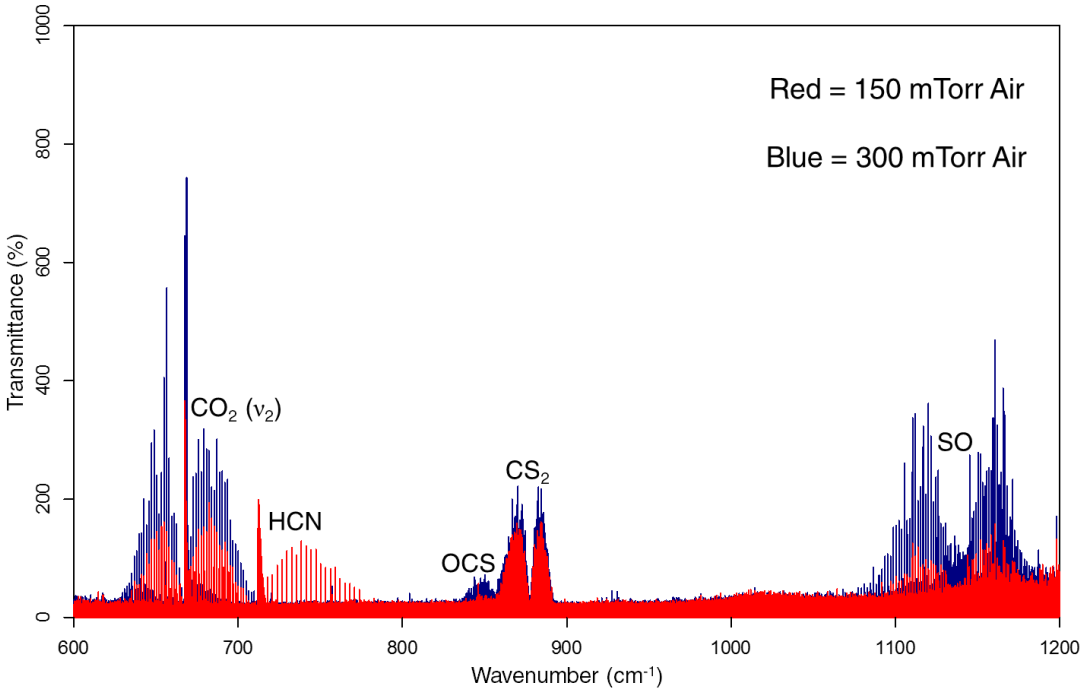

Figure 4.12: Comparison of Different Air Pressures (48 Scans Each)

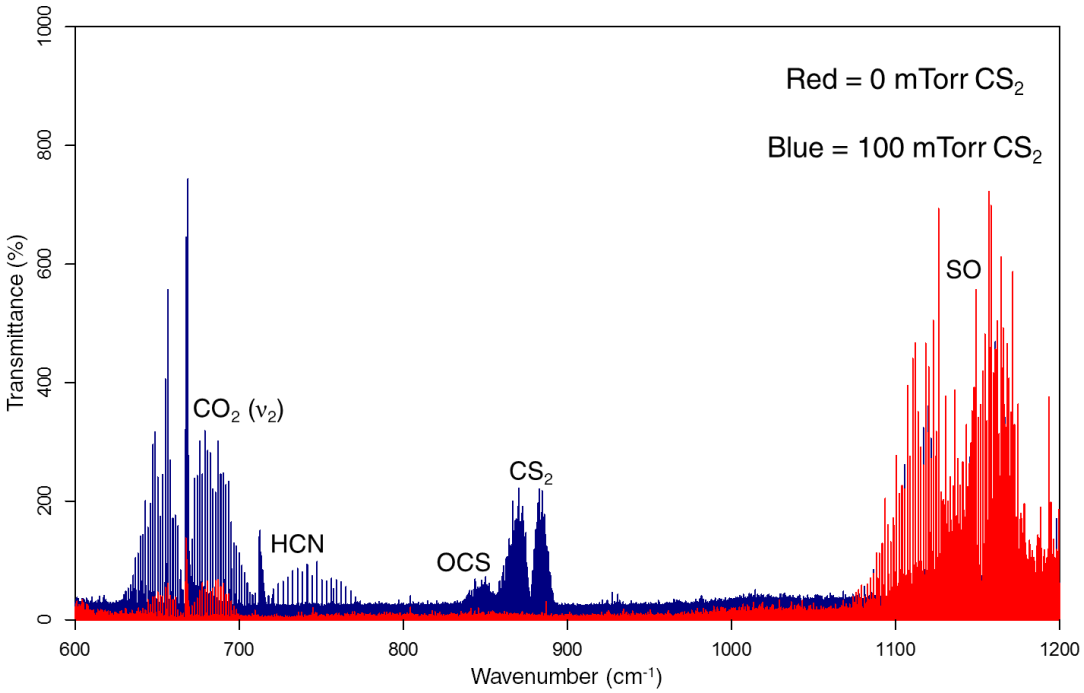

Figure 4.13: Comparison of Different CS_2 Pressures (32 Scans Each)

4.5.5 Effects of Reduced Voltage (Far/Mid-IR)

The reduced voltage spectrum (Figure 4.14) was recorded at a voltage setting of 2.00 kV. It should be noted that the default spectrum and reduced voltage spectrum have approximately the same level of noise; in Figure 4.14, it appears that the default has higher noise levels because the baselines are slightly offset. The reduction in discharge voltage managed to generate a new band in the spectrum: the ν_3 band (CH bend) of C_2H_2 at 729.16 cm^{-1}.[16] At the time, this was the longest molecule generated by the cell in a detectable amount and the closest to a chain (until SCCCS was uncovered in another spectrum at a higher frequency). Only the Q-branch of the C_2H_2 band was visible and the assignment was not pursued. The abundance of OCS in the cell was also increased, as both bands had higher intensities. As seen in Table 4.10, the ν_1 band of OCS also had an increase in the number of lines (100 to 115), the maximum J value (56 to 63) and most intense J value (24 to 26). The reduced voltage also decreased the intensities of the SO band and the non-fundamental CO_2 bands (many of which were too weak to assign). The number of observable lines of SO dropped significantly from 191 to 129 and the most intense J value shifted down from 18 to 16. As for the fundamental band of CO_2, the effect is not clear. The overall intensity of the band did drop a bit yet the number of observable lines increased from 47 to 65 while the maximum and most intense values remained the same. The abundances of CS_2 and HCN were relatively unaffected by the change in voltage with mostly minor changes to their band characters. The one significant change was the location of maximum intensity in the CS_2 band as it moved down from J = 32 to J = 24. Based on the results from this spectrum, it appears that lower voltage allows for larger molecules, like OCS and C_2H_2, to stabilize while higher voltages lead to more hot bands and an increased abundance of smaller, diatomic species (SO). This suggests that higher voltages lead to an increase in molecular destruction.

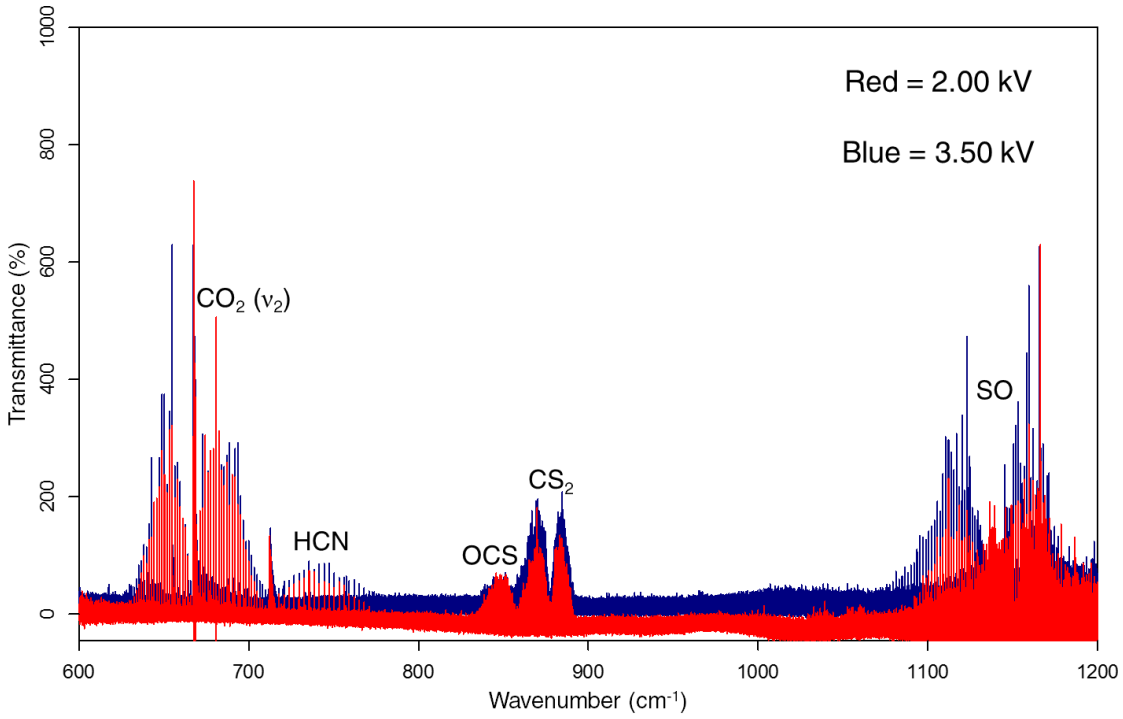

Figure 4.14: Comparison of Different Voltages (100 Scans Each)

4.5.5 Effects of Reduced Pumping Rate (Far/Mid-IR)

The final spectrum (Figure 4.15) was recorded after reducing the pumping rate throughput in half. As indicated by the saturation (note the lines below the baseline), the abundance of CO_2 and SO in the cell drastically increased. There appeared to be a decrease in the amount of HCN, OCS and CS_2 as the number of lines, maximum J values and most intense J values all decreased. At end of the spectral recordings, it was observed that the sample vial had nearly run dry of CS_2 which may have caused the decrease in the band strength of CS_2. As shown by the effects of removing CS_2 in an earlier spectrum (Figure 4.13), the reduction of the OCS and HCN bands were likely tied to the decrease of CS_2 in the cell. However, the increase in SO abundance does demonstrate that transient molecules could potentially benefit from a reduced pumping rate.

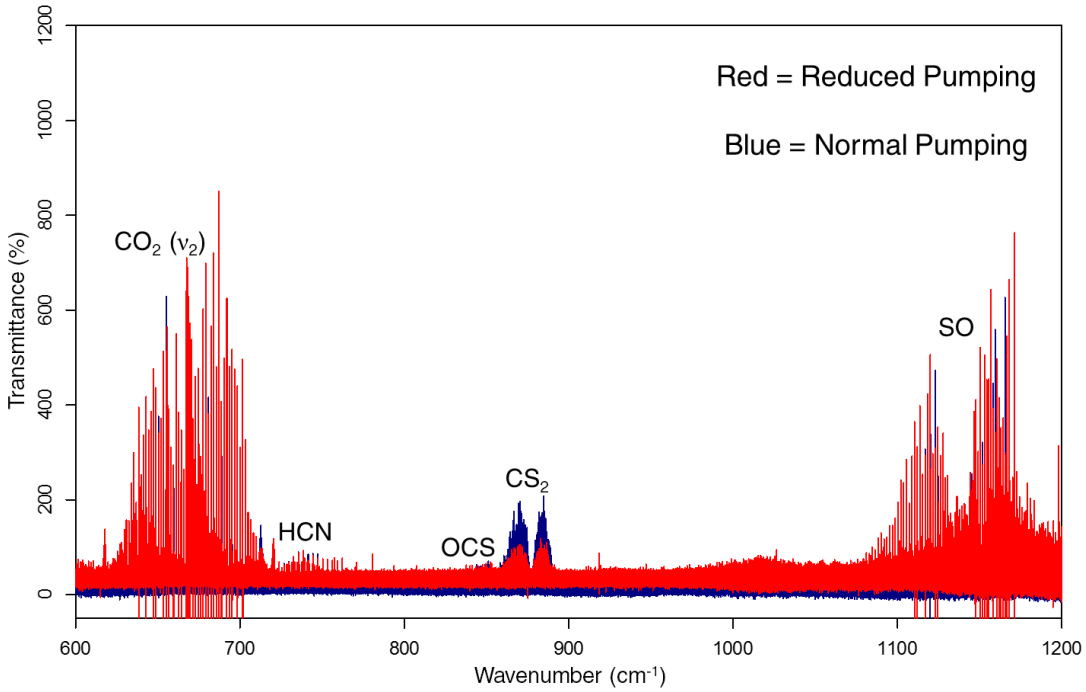

Figure 4.15: Comparison of Different Pumping Rates (100 Scans)

At this stage, additional optimization tests are still needed in order to propose stronger conclusions about the effects of discharge conditions. As one of the main goals in this project was to generate and study chain molecules, this experiment should be revisited and expanded but with the default voltage lowered to somewhere between 1.50 kV and 2.00 kV, the voltage range where SCCCS and C_2H_2 are known to stabilize. It would also be interesting to see what effect reduced pumping would have at this voltage settings and to see if it can assist in the detection of chain molecules. The next chapter discusses the performance of the cell and proposes ideas for future work that can be done with the new discharge cell.

4.6 References

[1] V. Ahrens and G. Winnewisser. *Z. Naturforsch.* **54a**, 131-136 (1999).

[2] S. Yamamoto, S. Saito, K. Kawaguchi, Y. Chikada, H. Suzuki, N. Kaifu, S. Ishikawa and M. Ohishi. *Astrophys. J.* **361**, 318-324 (1990).

[3] S. Yamamoto, S. Saito, K. Kawaguchi, N. Kaifu, H. Suzuki and M. Ohishi. *Astrophys. J.* **317**, L119-L121 (1987).

[4] V.D. Gordon, M.C. McCarthy, A.J. Apponi and P. Thaddeus. *Astrophys. J. Suppl. Ser.* **138**, 297-303 (2002).

[5] F. Holland, M. Winnewisser, C. Jarman, H.W. Kroto and K.M.T. Yamada. *J. Mol. Spectrosc.* **130**, 344-370 (1988).

[6] M.B. Bell, L.W. Avery and P.A. Feldman. *Astrophys. J.* **417**, L37-L40 (1993).

[7] T. Iino, A. Mizuno, T. Nakajima, T. Hidemori, T. Tsukagoshi and C. Kato. *Planet. Space Sci.* **104**, 211-215 (2014).

[8] K.M. Hickson, J.C. Loison, T. Cavalié, E. Hébrard and M. Dobrijevic. *A&A*. **572**, A58 (2014).

[9] R. I. Kaiser, C. Ochsenfeld, M. Head-Gordon and Y.T. Lee. *Science*. **279**, 1181-1184 (1998).

[10] M.A. Martin-Drumel, J. van Wijngaarden, O. Zingsheim, F. Lewen, M.E. Harding, S. Schlemmer and S. Thorwirth. *J. Mol. Spectrosc.* **307**, 35-39 (2015).

[11] J. Szczepanski, R. Hodyss, J. Fuller and M. Vala. *J. Phys. Chem.* **103**, 2975-2981 (1999).

[12] H. Wang, J. Szczepanski, P.J. Brucat and M.T. Vala. *J. Phys. Chem. A.* **107**, 10919-10925 (2003).

[13] H. Wang, J. Szczepanski, A. Cooke, P. Brucat and M. Vala. *Int. J. Quantum Chem.* **102**, 806-819 (2005).

[14] *OPUS*, version 7.0; Bruker Optik GmbH, 2011.

[15] C. Western, *PGOPHER: A Program for Simulating Rotational Structure*; University of Bristol, 2014. http://pgopher.chm.bris.ac.uk/

[16] T. Shimanouchi, *Tables of Molecular Vibrational Frequencies Consolidated Volume I*; National Bureau of Standards, 1972; pp 1-160.

[17] National Institute of Standards and Technology. NIST Atomic Spectra Database. http://www.nist.gov/pml/data/asd.cfm (accessed April 24, 2016).

[18] G. Herzberg, *Molecular Spectra and Molecular Structure II. Infrared and Raman Spectra of Polyatomic Molecules*, 2nd ed.; Krieger Publishing Company: Malabar, FL, USA, 1991.

[19] M.A. Martin-Drumel, S. Eliet, O. Pirali, M. Guinet, F. Hindle, G. Mouret and A. Cuisset. *Chem. Phys. Lett.* **550**, 8-14 (2012).

[20] E.K. Plyler, E.D. Tidwell and A.G. Maki, *J. Res. Nat. Bur. Stand.* **68A**, 79-86 (1964).

[21] F. Holland, M. Winnewisser, C. Jarman, H.W. Kroto and K.M.T Yamada. *J. Mol. Spectrosc.* **130**, 344-370 (1988).

[22] K. Jolma, J. Kauppinen and V.M. Horneman, *J. Mol. Spectrosc.* **101**, 300-305 (1983).

[23] J. Hietanen, K. Jolma and V.M. Hornenman, *J. Mol. Spectrosc.* **127**, 272-274 (1988).

[24] V.M. Horneman, M. Koivusaari, A.M. Tolonen, S. Alanko, R. Anttila, R. Paso and T. Ahonen, *J. Mol. Spectrosc.* **155**, 298-306 (1992).

[25] M. Dang-Nhu, G. Blanquet, J. Walrand and C.P. Courtoy, *Mol. Phys.* **58**, 995-1000 (1986).

[26] J.B. Burkholder, E.R. Lovejoy, P.D. Hammer and C.J. Howard, *J. Mol. Spectrosc.* **124**, 379-392 (1987).

Chapter 5: Final Remarks

The commissioning of a custom-built dc discharge cell designed for synchrotron-based far-IR spectroscopy has been completed and this cell is now the first of its kind in Canada. Optimization tests have been carried out to understand how best to operate the cell for the generation of transient molecules. While further optimization is needed to draw stronger conclusions, the data collected so far indicates that it is possible to study chain molecules of astrophysical interest using this cell with the Far-IR Beamline at the CLS. This chapter will go into more detail about the performance of the commissioned discharge cell and will provide suggestions for future work.

5.1 Evaluation of the Discharge Cell

The commissioning of the dc discharge cell was a success. The cell was able to generate and maintain a stable discharge for long periods of time (at least 10 hours per day) without any major problems. The discharge can be maintained at voltages as low as 0.40 kV and can withstand changes to the pumping rate. The discharge cell was used to collect high resolution rovibrational spectra in the far- and mid-IR regions as it is compatible with both synchrotron and globar radiation. Data collection in the far-IR region with SR can be conducted using the highest resolution setting of the beamline spectrometer (0.00096 cm^{-1}). The spectra revealed that the discharge cell was capable of generating transient molecules of astrophysical interest as both chains and diatomic radicals were detected. The design of the discharge cell has proven to be quite sturdy as no damage was incurred during the three rounds of beamtime. The cell remained unscathed during transportation, set up and throughout the experiments. As mentioned previously

in Chapter 3, the mirror protection system innovated for this project was also a success as solid discharge by-products were unable to reach the gold-coated mirrors in the end components of the cell thus keeping the mirrors clean.

One improvement that could be made to the discharge cell setup is to replace the high voltage power supply. A repurposed power supply provided by the CLS facility was used in this work and the electrical current readings on the display were not precise. It was not uncommon for the display to show that no current was running through the cell, even when the presence of a stable discharge plasma clearly indicated that there was. It would have been helpful to know what the current values actually were, especially during the optimization, as there are certainly some interesting correlations between the current and changes to the discharge conditions.

5.2 Future Work

As this project needed to be completed within the three weeks of beamtime granted by the CLS, there are many experiments and additional optimization tests that could be done in the future. Outlined in the following subsections are ideas and guidelines for future work with the commissioned discharge cell. An important piece of information gathered from the completed tests was that chain molecules can be generated in detectable concentrations at lower voltages of $\leq$2.00 kV and thus any future project concerned with these species should follow this direction.

5.2.1 Additional Optimizations

As mentioned in the previous chapter, the far-IR optimization tests used a higher voltage of 3.50 kV as one of the default settings. In retrospect, the high voltage likely prevented longer

chain molecules from forming in detectable quantities. These optimization tests should be repeated at a lower voltage of ≤2.00 kV in an effort to generate chains and determine if changes to other discharge conditions, such as pumping rate or sample pressures, can also help stabilize these species. In addition, these tests should be repeated for the mid-IR spectra as this region displays a different diversity of rovibrational bands than the far-IR region. There are many chain molecules, such as SCCCS, that have their strongest fundamental vibrational transitions in the mid-IR region. The detection and optimization of such bands in the mid-IR could assist in the generation of weaker fundamental transitions in the far-IR region. The optimal conditions for the far-IR transitions should be similar to those of the stronger mid-IR transitions. Spectral collection in the mid-IR region is much faster than in the far-IR region since the reduction in resolution (which is required due to the larger Doppler line widths) reduces scan times. Once a target band is optimized in the mid-IR region then the experiment can shift to the weaker transition in the far-IR region and a high resolution spectrum can be collected.

5.2.2 Carbon Subsulfide (SCCCS)

Conducting optimizations using low voltage in the mid-IR region should hopefully grant some insight into the best method for generating SCCCS. The strongest transition for this molecule is the ν_3 band (C-S antisymmetric stretch)[1] located at 2100 cm^{-1}, which was used to positively identify SCCCS in the early test spectra. If this band can be strengthened significantly, then it may be possible to detect the weaker ν_4 band (C-C antisymmetric stretch) at 1030 cm^{-1}. According to B3LYP/6-311++G(2d,2p) and MP2/6-311++G(2d,2p) *ab initio* calculations carried out in this work using Gaussian 09,[2] the ν_4 band of SCCCS should be about 1/10 to 1/7 of the strength of the ν_3 band (simulated spectrum in Figure 5.1). The only known high resolution studies

of SCCCS have focused solely on the ν_3 band system.[3,4] If the ν_3 band can be detected and optimized using the commissioned discharge cell, then the first high resolution study of the ν_4 band system may be possible. Additionally, a successful study of SCCCS may lead to the detection of a related chain molecule: OCCCS (recall that OCS was also detected in the discharge cell). The strongest transition for this species is the ν_3 band (C-S/C-O antisymmetric stretch) located at 2240 cm^{-1}.[3] However, *ab initio* calculations from this work (same methods and basis sets as before) indicate that it may be difficult to detect the far-IR transitions which are predicted to be no more than 1/100 of the strength of the ν_3 band.

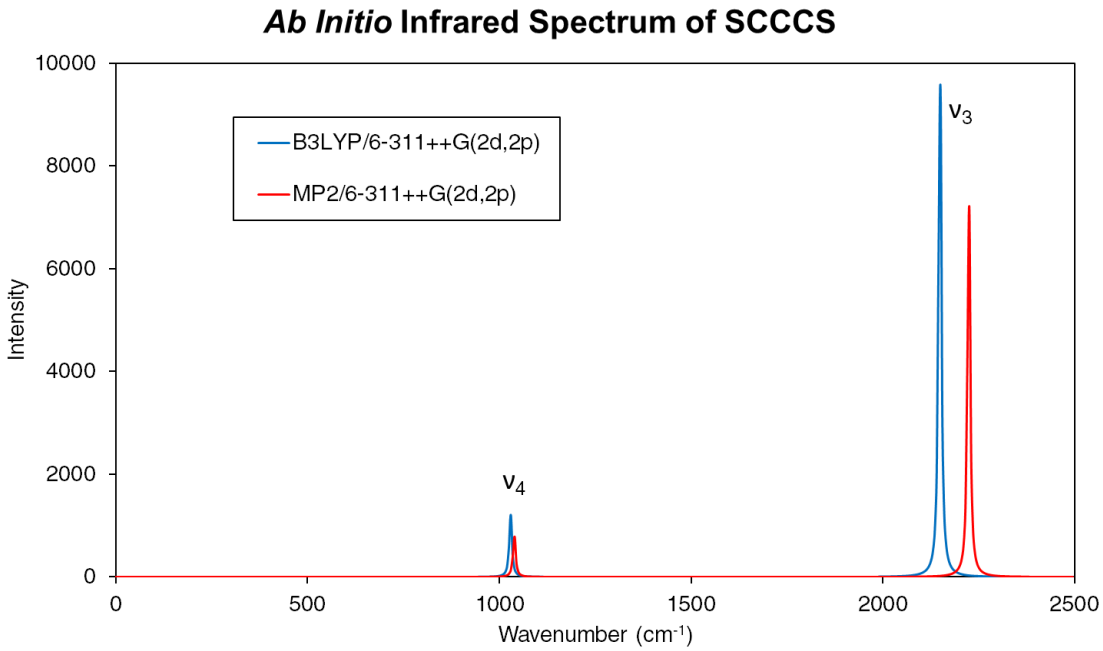

Figure 5.1: Simulated Infrared Vibrational Spectrum of SCCCS

5.2.3 Further Experiments with CS_2

A yet-to-be-achieved objective for this project is the generation and detection of C_xS chains ($x > 1$) formed in the discharge of CS_2. Due to their structural similarities, the detection of SCCCS has confirmed that the formation of C_xS chains is possible using the commissioned discharge cell although these molecules are highly unstable as they are diradicals. In addition to the use of high voltage, the problem may be that the precursor mixture used did not contain enough carbon sources. In previous studies of C_xS chains that used electric discharge in a pulsed supersonic jet, CS_2 was mixed with C_2H_2 or C_4H_2 and voltages were set within the range of 1.30 to 1.90 kV.[5,6] It should also be noted that these chains have only been detected in microwave[5,6] and mid-IR regions,[7,8] the latter of which was done with laser ablation rather than electric discharge. Currently, there are no known high resolution studies of these chains in the far-IR region.

5.2.4 Other Precursors

The detection of cyano-bearing molecules in astronomical objects is of great interest to astronomers who seek out signs of life in space. This is because the cyano-bearing molecules are involved in reactions that build biological matter such as amino acids.[9] Many cyano-bearing molecular chains of the form HC_xN ($x>2$) have been found in various regions of the ISM[10-12] and in comets.[13] In FTMW studies using electric discharge in a pulsed jet discharge, longer forms of these chains ($17>x>3$) were generated by discharging HC_3N (which is commercially available) with C_4H_2 and voltage settings in the range of 1.40 to 1.90 kV.[14-16] So far, there are no known studies of HC_xN chains in the far-IR regions, or even any mid-IR studies for $x>5$ chains, so the study of the discharge of HC_3N using the commissioned discharge cell may prove to be ground-breaking.

Like sulfur, silicon has been found in nearly 10% of the known species in the ISM.[17] Additionally, certain silicon-bearing diatomic radicals have been detected in meteorites,[18] the Sun[19] and Earth's moon.[20] Discharge techniques have been used to produce silicon-bearing transient molecules ranging from diatomic radicals to long chains. At least four different forms of silicon-bearing chains have been observed in the microwave and mid-IR regions: SiC_x,[21] SiC_xH,[22] SiC_xSi,[23] SiC_xS.[24] None of these four types of chain species have been detected in the far-IR region and certain diatomic species (SiBr, SiCl, SiN) have yet to be studied using infrared spectroscopy. Common precursors used to generate silicon-bearing transient species are $SiCl_4$ for diatomics and SiH_4 for chains. However, SiH_4 is quite hazardous to work with whereas $SiCl_4$ is relatively safe. Therefore, a possible experiment to try with the commissioned discharge cell is to innovate a way to form silicon-bearing chains using the $SiCl_4$ precursor. Adding CS_2 to $SiCl_4$ could potentially form SiC_xS chains while the addition of C_2H_2 or C_4H_2 could be used for SiC_x, SiC_xSi or SiC_xH chains. As some of the discharge by-products will contain chlorine, the cold trap would need to be well-maintained.

There are many more transient molecules that one could attempt to generate and study using the commissioned discharge cell. These laboratory studies of transient molecules are important to astronomers as many transient species naturally exist and are stable in various regions of space. As mentioned in Chapter 1, the identification of molecular emissions from astronomical objects requires the availability of relevant laboratory data, especially spectra collected using FTMW and FTIR techniques. However, the lack of high resolution techniques available in the far-IR region has impeded the availability of reliable spectroscopic data in that region. This is why it is so important to study molecules of astrophysical interest using far-IR beamlines at synchrotrons. The commissioned discharge cell built for this project now allows for users to study

transient molecules using the Far-IR Beamline at the Canadian Light Source. This is now the second facility in the world to allow for this type of spectroscopic study and may be the first to publish a high resolution study of a long chain molecule in the far-IR region.

5.3 References

[1] F. Holland, M. Winnewisser, C. Jarman, H.W. Kroto and K.M.T. Yamada. *J. Mol. Spectrosc.* **130**, 344-370 (1988).

[2] Gaussian 09, Revision B.01, M. J. Frisch, G. W. Trucks, H. B. Schlegel, G. E. Scuseria, M. A. Robb, J. R. Cheeseman, G. Scalmani, V. Barone, B. Mennucci, G. A. Petersson, H. Nakatsuji, M. Caricato, X. Li, H. P. Hratchian, A. F. Izmaylov, J. Bloino, G. Zheng, J. L. Sonnenberg, M. Hada, M. Ehara, K. Toyota, R. Fukuda, J. Hasegawa, M. Ishida, T. Nakajima, Y. Honda, O. Kitao, H. Nakai, T. Vreven, J. A. Montgomery, Jr., J. E. Peralta, F. Ogliaro, M. Bearpark, J. J. Heyd, E. Brothers, K. N. Kudin, V. N. Staroverov, T. Keith, R. Kobayashi, J. Normand, K. Raghavachari, A. Rendell, J. C. Burant, S. S. Iyengar, J. Tomasi, M. Cossi, N. Rega, J. M. Millam, M. Klene, J. E. Knox, J. B. Cross, V. Bakken, C. Adamo, J. Jaramillo, R. Gomperts, R. E. Stratmann, O. Yazyev, A. J. Austin, R. Cammi, C. Pomelli, J. W. Ochterski, R. L. Martin, K. Morokuma, V. G. Zakrzewski, G. A. Voth, P. Salvador, J. J. Dannenberg, S. Dapprich, A. D. Daniels, O. Farkas, J. B. Foresman, J. V. Ortiz, J. Cioslowski, and D. J. Fox, Gaussian, Inc., Wallingford CT, 2010.

[3] F. Holland, M. Winnewisser, C. Jarman, H.W. Kroto and K.M.T Yamada. *J. Mol. Spectrosc.* **130**, 344-370 (1988).

[4] F. Holland and M. Winnewisser. *J. Mol. Spectrosc.* **147**, 496-512 (1991).

[5] V.D. Gordon, M.C. McCarthy, A.J. Apponi and P. Thaddeus, *Astrophys. J. Suppl. Ser.* **134**, 311-317 (2001).

[6] Y. Kasai, K. Obi, Y. Ohshima, Y. Hirahara, Y. Endo, K. Kawaguchi and A. Murakami, *Astrophys. J.* **410**, L45-L47 (1993).

[7] H. Wang, J. Szczepanski, A. Cooke, P. Brucat and M. Vala, *Int. J. Quantum Chem.* **102**, 806-819 (2005).

[8] H. Wang, J. Szczepanski, P. Brucat and M. Vala, *J. Phys. Chem. A.* **107**, 10919-10925 (2003).

[9] D. Rehder, *Chemistry in Space: From Interstellar Matter to the Origin of Life*; Wiley-VCH Verlag GmbH & Co. KGaA: Weinheim, Germany, 2010.

[10] R. L. Snell, F.P. Schloerb, J. S. Young, A. Hjalmarson and P. Friberg, *Astrophys. J.* **244**, 45-53 (1981).

[11] J. Cernicharo, R. Bachiller and G. Duvert, *Astron. Astrophys.* **160**, 181-184 (1986).

[12] M.B. Bell, P.A. Feldman, S. Kwok and H.E. Matthews, *Nature*, **295**, 389-391 (1981).

[13] D. Bockelée-Morvan and J. Crovisier, *Earth Moon Planets*. **89**, 53-71 (2002).

[14] M.C. McCarthy, E.S. Levine, A.J. Apponi and P. Thaddeus, *J. Mol. Spectrosc.* **203**, 75-81 (2000).

[15] M.J. Travers, M.C. McCarthy, P. Kalmus, C.A. Gottlieb and P. Thaddeus, *Astrophys. J.* **472**, L61-L62 (1996).

[16] M.C. McCarthy, J.U. Grabow, M.J. Travers, W. Chen, C.A. Gottlieb and P. Thaddeus, *Astrophys. J.* **494**, L231-L234 (1998).

[17] H.S.P. Muller, M.C. McCarthy, L. Bizzochi, H. Gupta, S. Esser, H. Lichau, M. Caris, F. Lewen, J. Hahn, C. Degli Esposti, S. Schlemmer and P. Thaddeus, *PCCP.* **9**, 1579-1586 (2007).

[18] A.C. Andersen, C. Jäger, H. Mutschke, A. Braatz, D. Clément, T. Henning, U.G. Jørgensen and U. Ott, *Astron. Astrophys.* **343**, 933-938 (1999).

[19] D.A. Glenar, A.R. Hill, D.E. Jennings and J.W. Brault, *J. Mol. Spectrosc.* **111**, 403-414 (1985).

[20] D.D. Cudaback, J.E. Gaustad and R.F. Knacke, *Astrophys. J.* **166**, L49-L51 (1971).

[21] M.C. McCarthy, A.J. Apponi, C.A. Gottlieb and P. Thaddeus, *Astrophys. J.* **538**, 766-772 (2000).

[22] M.C. McCarthy, A.J. Apponi, C.A. Gottlieb and P. Thaddeus, *J. Chem. Phys.* **115**, 870-877 (2001).

[23] J.D. Presilla-Márquez, C.M.L. Rigby and W.R.M. Graham, *J. Chem. Phys.* **106**, 8367-8373 (1997).

[24] P. Botschwina, M.E. Sanz, M.C. McCarthy and P. Thaddeus, *J. Chem. Phys.* **116**, 10719-10729 (2002).